EUROPEAN ORGANIZATION FOR NUCLEAR RESEARCH (CERN)

CERN-EP-2019-266
2020/06/15

CMS-PRF-18-003

Measurements with silicon photomultipliers of dose-rate effects in the radiation damage of plastic scintillator tiles in the CMS hadron endcap calorimeter

The CMS Collaboration*

arXiv:2001.06553v2 [physics.ins-det] 11 Jun 2020

Abstract

Measurements are presented of the reduction of signal output due to radiation damage for two types of plastic scintillator tiles used in the hadron endcap (HE) calorimeter of the CMS detector. The tiles were exposed to particles produced in proton-proton (pp) collisions at the CERN LHC with a center-of-mass energy of 13 TeV, corresponding to a delivered luminosity of 50 fb^{-1}. The measurements are based on readout channels of the HE that were instrumented with silicon photomultipliers, and are derived using data from several sources: a laser calibration system, a movable radioactive source, as well as hadrons and muons produced in pp collisions. Results from several irradiation campaigns using ^{60}Co sources are also discussed. The damage is presented as a function of dose rate. Within the range of these measurements, for a fixed dose the damage increases with decreasing dose rate.

"Published in the Journal of Instrumentation as doi:10.1088/1748-0221/15/06/P06009."

© 2020 CERN for the benefit of the CMS Collaboration. CC-BY-4.0 license

*See Appendix A for the list of collaboration members

1 Introduction

Because of their versatility and low cost, plastic scintillators are used in the construction of detectors built for experiments at particle colliders. They are, however, subject to a reduction in their signal output after irradiation (radiation damage) [1]. Two of the hadron calorimeters (HCAL) of the CMS detector [2] —the hadron barrel (HB) [3] and the hadron endcap (HE) [4]— at the CERN LHC [5] use tiles constructed from plastic scintillator with embedded wavelength shifting (WLS) fibers to produce their signals. There are also plans to use scintillators in the CMS endcap calorimeters upgraded for the high-luminosity LHC runs [6].

This paper presents results on the reduction of signal collected from irradiated scintillator tiles as a function of dose rate R. These results provide unique information about radiation damage at dose rates significantly lower than previously studied. The HE tiles, described in Sec. 3, and their associated fibers, were irradiated by particles produced in pp collisions at the LHC during 2017 at a center-of-mass energy of 13 TeV, corresponding to a delivered luminosity of $50\,\text{fb}^{-1}$. The R range is extended by including studies of tiles placed in a moderate-R region of the CMS collision hall forward of the HE, as well as tiles irradiated using external high-dose-rate ^{60}Co sources. The reliability of the measurements is improved by using tiles that were instrumented before the 2017 data-taking period with silicon photomultipliers (SiPMs, also known as Geiger Mode Silicon Avalanche Photodiodes). The HE tile results are obtained using several complementary methods. We use a movable radioactive source that can access all the tiles to compare their signal output before and after the 2017 data-taking period. Inclusive energy deposits from pp collisions and energy deposits by isolated muons are also used to monitor the signal output. In addition, some of the HE tiles and the tiles in the moderate-R region of the collision hall are studied using a laser calibration system. The results indicate an R-dependent effect; scintillators receiving the same ionizing dose at different dose rates have different reductions in collected signal.

This study supersedes our previous results [7], which were based on data collected in 2016 using hybrid photodiodes (HPDs) as the photodetectors. Those photodetectors were subsequently shown to have suffered significant response degradation over the course of the running period because of damage to the photocathodes by ion feedback [8], and not to radiation damage. In the previous publication [7], the reduction of signal output was attributed solely to radiation damage to the scintillator tiles.

This paper is organized as follows. In Section 2, we summarize what is known about radiation damage mechanisms in plastic scintillators. In Section 3, we give a brief description of the CMS detector, and a more detailed description of the HE calorimeter. In Section 4, we present measurements of radiation damage to the tiles embedded within the HE. The calculation of the dose is described, followed by the results obtained using a laser calibration system to monitor the signal loss, and using a radioactive source for this purpose. A parametrization of the R dependence is given. The signal loss observed in response to hadrons during collisions is studied for consistency with the laser results, and the signal loss in response to muons is also shown. In Section 5, we present studies of dose-rate effects measured outside of the CMS detector using irradiation by sources as well as studies using tiles in the moderate-radiation zone of the CMS collision hall. In Section 6, we summarize other relevant information and discuss the dose-rate effects. Finally, in Section 7, we present a summary and the conclusions of the paper.

2 Radiation damage mechanisms

For the purpose of our studies, we refer to the HCAL tiles as objects consisting of plastic scintillator, a WLS fiber, a Tyvek^{TM} wrapping, a clear fiber, and a transducer. Our estimates, presented below, indicate that the contribution from WLS fibers to the overall signal loss is small, and the contributions from clear quartz fibers, Tyvek^{TM} wrappers and the SiPM transducers are negligible. Consequently, we believe that our results represent primarily the damage to the scintillator tiles.

Plastic scintillators consist of a plastic substrate, often polystyrene (PS) or polyvinyltoluene (PVT), into which fluorescent agents (fluors) have been dissolved, usually a primary and a secondary fluor. When a charged particle traverses the scintillator, the molecules of the substrate are excited. This excitation can be transferred to the primary fluor via the Förster mechanism [9] at primary fluor concentrations above approximately 1% [10]. The primary fluor transfers the excitation radiatively to the secondary fluor. For the HCAL tiles made of SCSN−81, a PS-based scintillator from Kuraray[1], the absorption maximum of the primary fluor is at the wavelength of approximately 280 nm, and the emission is approximately at 320–350 nm. The absorption maximum of the secondary fluor corresponds to the emission maximum of the primary fluor, and the de-excitation of the secondary fluor has a wavelength of maximum emission of approximately 440 nm (blue light). This visible light must traverse the scintillator to reach the WLS fiber, and can be reduced by imperfections in the material (color centers) along its path.

Generally, the scintillator signal output decreases exponentially with the dose received, as expected for light attenuation due to radiation-induced color centers; this behavior was also observed in source measurements [4], which were used to design the HCAL optics:

$$L(d) = L_0 \exp(-d/D) = L_0 \exp(-d\,\mu), \tag{1}$$

where $L(d)$ is the signal output after receiving a dose d, L_0 is the signal output before irradiation, μ is a function that depends on the dose rate R, and $D = 1/\mu$. When the damage is small compared to measurement uncertainties, D fluctuates to large positive or negative numbers. Therefore μ is used to fit the data and evaluate the uncertainties. The fitted values of μ can be averaged over bins of dose rate to improve statistical accuracy. The $\langle\mu\rangle$ results are used to parametrize the R dependence (D is shown in some figures of this paper).

The value of μ depends on the materials used in the fabrication of the scintillator and on how it is handled (e.g., if it comes into contact with oils, etc.) prior to and during experimental operations. Several results have been presented on the dependence on dose rate [7, 11–18]. In Refs. [17], the authors saw no change in the signal output or attenuation length for SCSN−81 down to dose rates of 2 Gy/h, whereas the authors of Refs. [11, 12] saw effects at dose rates between 10 Gy/h and 10 kGy/h. A review of the causes of dose-rate effects, and particularly the prominent role played by the diffusion of oxygen and polymer oxidation, is given in Section 6.

Damage to the fluors can occur [13], but it is generally small [16, 19]. Damage to the substrate often results in the creation of radicals, conjugated double bonds, carbonyl species formed by reaction with oxygen, and trapped electrons, and other structures that can be color centers. Color centers that interfere with the transfer of light between the primary and secondary fluors reduce the initial light yield. Color centers that absorb the light output by the secondary fluor reduce the absorption length of the light in the scintillator.

Radicals are produced when chemical bonds in the polymer are broken. The bonds can re-form on a time scale that depends on such factors as the density of the radicals and the temperature.

[1] Kuraray, Ote Center Building, 1-1-3, Otemachi, Chiyoda-ku, Tokyo 100-8115, Japan

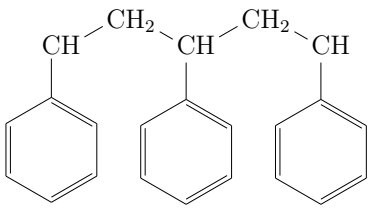

Figure 1: Polystyrene.

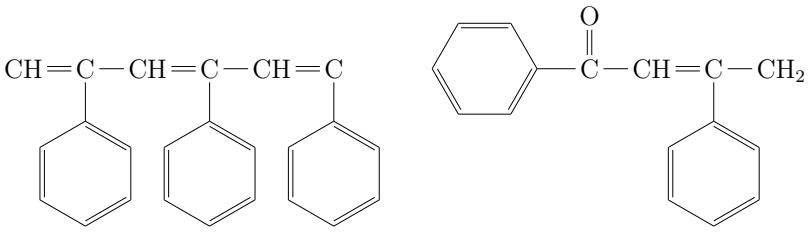

Figure 2: Examples of changes to polystyrene undergoing irradiation. The change on the right can only occur in the presence of oxygen.

Such damage is called temporary damage, and the re-forming of bonds is known as annealing. Some products cause permanent changes in the chemical structure. Figure 1 shows the chemical structure of unirradiated PS. Figure 2 shows some of the permanent color centers that can be formed in PS [20].

3 CMS detector

The central feature of the CMS apparatus is a superconducting solenoid of 6 m internal diameter, providing a magnetic field of 3.8 T. Within the solenoid volume are silicon pixel and strip trackers, a lead tungstate crystal electromagnetic calorimeter (ECAL) composed of a barrel and two endcap sections, an endcap preshower, and the HB and HE.

The silicon tracker measures charged particles within the pseudorapidity range $|\eta| < 2.5$. It consists of 1440 silicon pixel and 15 148 silicon strip detector modules. Isolated particles of transverse momentum $p_{\mathrm{T}} = 100\,\mathrm{GeV}$ emitted at $|\eta| < 1.4$ have track resolutions of 2.8% in p_{T} and 10 (30) μm in the transverse (longitudinal) impact parameter [21]. Muons are measured in the range $|\eta| < 2.4$, with detection planes embedded in the steel flux-return yoke outside the solenoid that are made using three technologies: drift tubes, cathode strip chambers, and resistive plate chambers.

A more detailed description of the CMS detector, together with a definition of the coordinate system used and the relevant kinematic variables, can be found in Ref. [2]. A description of the CMS trigger system can be found in Ref. [22].

The scintillator tiles that exhibit damage are located in the HE, which has 18 layers of active material, denoted layers 0 through 17, over most of its η coverage. The zeroth layer of scintillator uses BC$-$408, a PVT-based scintillator from the Bicron division of the Saint-Gobain corpora-

tion[2], while the other layers use PS-based SCSN−81. Scintillators based on PVT are brighter than those based on PS.

The scintillator tiles are optically isolated. They are trapezoidal in shape, and their faces have a groove shaped like the Greek letter σ that holds a 0.94 mm-diameter Y−11 (Kuraray) WLS fiber, mirrored on one end. The tiles are wrapped in Tyvek^{TM}. Clear quartz fibers attached to the WLS fibers lead to the photodetectors. Quartz fibers are well known to be radiation hard. In CMS, we observe small radiation damage to quartz fibers embedded in the Hadron Forward calorimeter, which is located in a much higher radiation environment than the HE. The impact of radiation on the Tyvek^{TM} wrapping is discussed in Sec. 5 and is shown to be negligible. The tile thickness is 0.9 cm in layer 0 and 0.37 cm in the rest of the layers. When the HE was designed, a thicker and brighter scintillator in layer 0 was chosen in an attempt to mitigate the noncompensating response of the ECAL to hadrons and the large amount of dead material installed before the HE for ECAL readout.

The HE geometry is projective in η-ϕ-z space, where ϕ is the azimuth and z is the coordinate along the beam line, with the origin of the coordinate system positioned at the nominal collision point. Tiles in successive layers are aligned in a "tower". The towers are labeled using integer indices based on their η and ϕ. For the HE, the $i\eta$ index ranges from 16 to 29, covering $1.305 < |\eta| < 3$. The $i\phi$ index ranges from 1 to 72, with $i\phi = 1$ halfway up the detector and 18 and 19 at its top. A tower corresponds to the hardware associated with an $i\eta$-$i\phi$ pair. The tiles are mounted as mechanical structures called megatiles, shown in Fig. 3, which in the HE are installed in layers perpendicular to the beam direction, and span the range of 400–550 cm in $|z|$ and 40–260 cm in radius, depending on z.

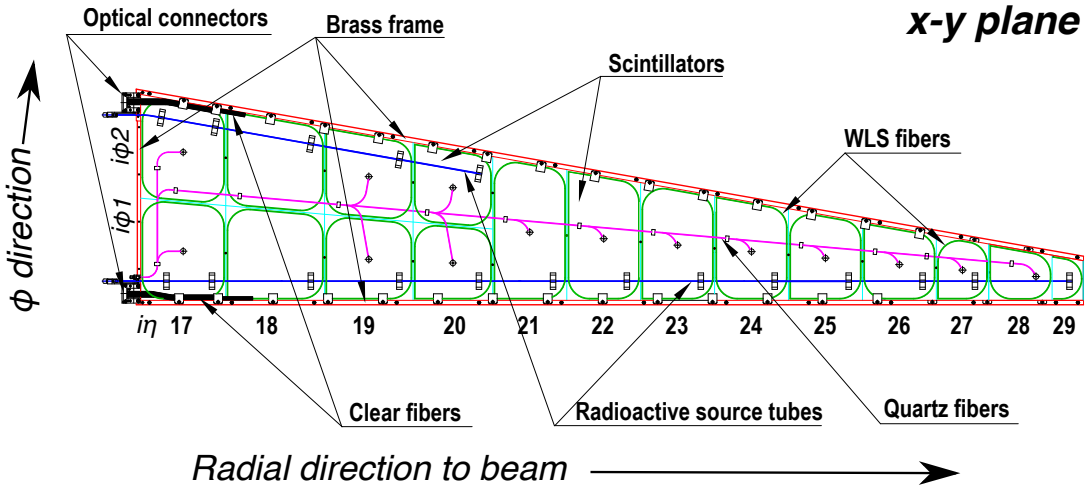

Figure 3: Details of an HE megatile showing the scintillator tiles, the WLS fibers, and the clear readout fibers. Also shown are the quartz fibers, which carry the laser light and the tubes through which the radioactive source moves. In layer 1, the inner size of the megatile is around 7.3 cm, while the outer size is 38.5 cm and the radial extent is 175 cm. The sizes (the longer base and the height) of enclosing trapezoids vary between 9.6 cm × 12.1 cm for the smallest ($i\eta = 27$), and 13.6 cm × 26.5 cm for the largest ($i\eta = 21$) tile used in this analysis.

[2]Saint Gobain Corp, Les Miroirs, 18, avenue d'Alsace, 92400 Courbevoie, France

To limit the number of readout channels, the light from several layers in a tower is fed to the same photodetector. In the schematic of the HE shown in Fig. 4, layers that are fed to a single SiPM have the same color ("depth").

For data taking prior to 2017, HPDs were used as the HE photodetector [23]. For the 2017 data-taking period, tiles in HE towers with $i\phi$ indices of 63–66, corresponding to a 20° sector in ϕ, were read out using SiPMs. Our analysis is based on $i\phi$s 63 and 65, because the other $i\phi$s only probed $i\eta$s below 20 where the radiation damage is too small to be measured reliably.

The HE SiPMs have 2–3 times greater quantum efficiency and better lifetime response stability than HPDs, no magnetic field sensitivity, require only medium voltage ($\approx$ 70 V) biasing, have small physical size, and allow the readout of more detector fibers supporting improved longitudinal segmentation. The SiPMs are placed at large radii in the HE, and receive a small radiation dose. Test bench measurements of SiPMs irradiated with radioactive sources showed [24] that the effect of 2017 radiation fluences on the HE SiPM response is negligible. Unlike the HPDs [8], their gain does not decrease because of light signals received from the tiles. The primary challenge for SiPM operation is the relatively high dark current resulting from cumulative radiation damage to the devices in situ during future running of high-luminosity LHC.

The CMS HCAL SiPM devices [25] are fabricated by the Hamamatsu Corporation[3]. The approximate device parameters are 15 μm pixel pitch, 4500 pixels per mm^2, 8 ns pixel recovery time, and 65 V breakdown voltage. We operate the SiPMs in the Geiger mode at an overvoltage of approximately 3 V, which corresponds to an operating voltage of about 68 V. This value was chosen because it maximizes the signal-to-noise ratio. At this operating voltage, the performance parameters are approximately 40 fC per single photoelectron, 12% pixel crosstalk, and 28% photon detection efficiency. Two sizes of circular SiPMs are used: 2.8 mm diameter devices for depths with four or fewer scintillator layers and 3.3 mm devices for the other depths.

A charge-integrating ASIC (QIE) [26] is used to read out, digitize, and encode the signals from the photodetectors.

Radiation damage to scintillators is sensitive to temperature. The temperature in the CMS collision hall is about 18° C.

4 Results from radiation exposure during pp collision data taking

The primary characteristics of the LHC operation relevant for this analysis are the total delivered luminosity, which determines the doses received by the tiles, and the average luminosity delivered per hour, which controls the dose rates. The integrated luminosity delivered as a function of time as well as the daily maximum instantaneous luminosity in the CMS interaction region in 2017 are displayed in Fig. 5. The daily peak luminosity rose rapidly and then remained at an approximately constant value throughout the year. The mean number of interactions per bunch crossing was about 37. Multiple interactions present in the recorded beam-beam crossing (event) are referred to as pileup.

4.1 Estimation of doses and dose rates in the HE tiles

For a given luminosity, a tile is subjected to a dose and dose rate that depend on its location in the detector. The doses and dose rates vary with pseudorapidity, following the particle energy density of the pp collisions, and with depth in the calorimeter, following the energy deposition profile of the electromagnetic and hadron showers.

[3] Hamamatsu Corporation, 325-6, Sunayama-cho, Naka-ku, Hamamatsu City, Shizuoka Pref., 430-8587, Japan

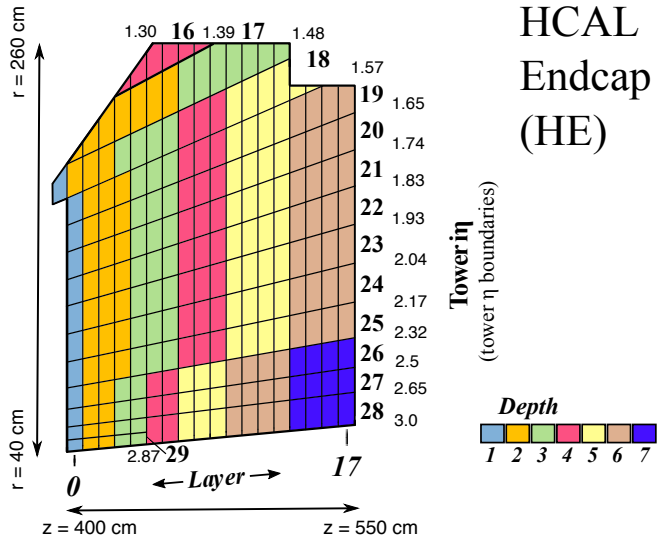

Figure 4: Schematic of the readout segmentation of the HE for channels instrumented with SiPMs. Scintillator tiles within a tower that have the same color ("depth") are connected to a single photodetector. The numbers 0–17 refer to the scintillator layers, and the numbers 16–29 on the perimeter of the figure denote the $i\eta$ indices of the towers (the η values for the boundaries of the towers are also shown).

The dose received by each HE scintillator tile per pp interaction is calculated using simulation and scaled according to the delivered luminosity. The calculated doses are verified by in situ dosimetry. The peak luminosity versus time was fairly flat during 2017 data taking, indicating stable running conditions, as shown in Fig. 5 (lower). We therefore calculate the average integrated luminosity delivered per hour for the whole data-taking period as follows: for the total of 50 fb^{-1} taken over $\approx$1670 h of interacting beams we obtain an average integrated luminosity of 0.03 fb^{-1}/h, with an estimated systematic uncertainty of 5%. This value is converted to a dose rate (in Gy/h) for every HE tile by multiplying the average luminosity per hour by the expected dose per 1 fb^{-1}.

Predictions of the absorbed dose in the HE scintillator layers are obtained using the Monte Carlo code FLUKA 2011.2c [27, 28]. The FLUKA predictions for collisions use a model that represents the HE in detail, with brass, Dural$^{\text{TM}}$ (Al, Cu, Mg, and Mn), Tyvek$^{\text{TM}}$, air, and scintillator layers. Since the energy loss per unit mass is more than a factor of two higher for hydrogen than for most other materials, and since plastic has a high hydrogen content, the spatial resolution in the simulation is set so that the dose estimates for tiles does not include regions that are not plastic. Per 50 fb^{-1}, doses in layer 1 range between 0.03 and 6 kGy for $i\eta$ of 18 to 29; for layer 7 they range between 0.003 to 0.7 kGy for $i\eta$ of 18 to 28. Layers 1 and 7 are located at $z = 410$ and 463 cm, respectively. The calculated doses for the 2017 running period for the tiles in layers 1 and 7 are presented in Fig. 6.

The calculated doses are verified using measurements with 24 FWT-60 series film dosimeters, from Far West Technologies[4] that were installed in the gaps between the absorber and the megatiles in the HE detector layers 1 and 2 during the 2015 and 2016 data-taking periods,

[4]Far West Technologies, 330 South Kellogg Ave., Suite D, Goleta, CA 93117 USA

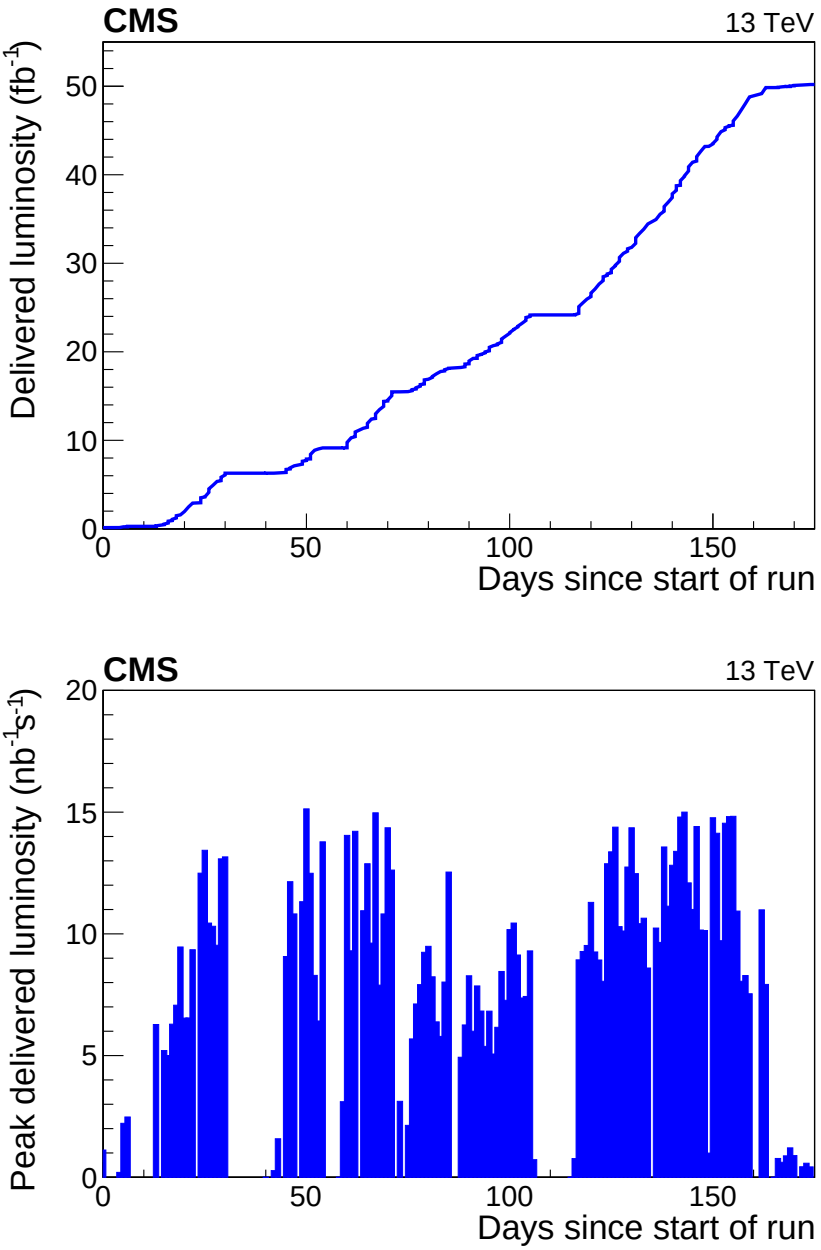

Figure 5: Integrated luminosity delivered to CMS by the LHC in the 2017 pp data-taking period, as a function of time (upper) and maximum daily (peak) luminosity delivered to CMS in 2017 (lower). Intervals of constant luminosity in the upper plot, or with no entries in the lower plot, indicate periods with no beam, e.g., technical stops.

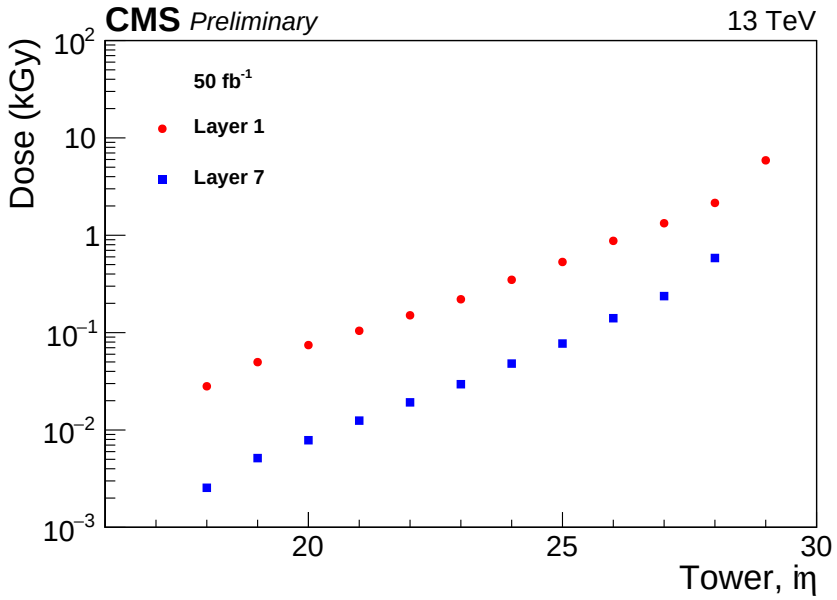

Figure 6: Doses calculated by FLUKA for the HE tiles in layers 1 and 7 as a function of $i\eta$ for 50 fb^{-1} of LHC running at 13 TeV in 2017.

when the detector geometry was essentially the same as in 2017. The films were measured with a FWT-92D photometer. The doses were calibrated to water equivalent, which is similar to plastic in terms of density and hydrogen content, and the uncertainty in the measurements is estimated to be 3%. A comparison between the measured and calculated doses as a function of the distance from the beam line to the film is given in Fig. 7. Reasonable agreement is seen for radial distances starting at about 50 cm, the location of tower $i\eta = 28$, indicating that FLUKA calculation is accurate to about 20–30% for distances 50–120 cm from the beam, where the largest radiation damage occurs for the tiles used in this analysis.

The geometry of the detector near towers 28 and 29 is irregular and the dose distribution difficult to model accurately (due to close proximity to the beam line, beam spray effects, irregular edges of the endcap preshower and electromagnetic calorimeter, mounting brackets and other construction elements, piping, etc.). For this reason, data taken for towers 28 and 29 are not included in the fits, although they are presented in some of the figures below.

4.2 Results using the laser calibration system

A laser calibration system is used to monitor the response of the HE tiles by injecting ultraviolet (UV) light that excites primary fluors in the scintillator. It consists of a triggerable excimer laser and a light distribution system that delivers UV light (351 nm) to the scintillator tiles in layers 1 and 7 via quartz fibers. During the 2017 data-taking period, pulses of laser light were injected between fills of the accelerator with protons, when there were no collisions.

Laser data were collected throughout the 2017 data-taking period. Figure 8 shows the signal output for the tiles probed by the laser calibration system at the end of the 2017 data-taking period relative to that at the start. Because the intensity of the laser light varied by up to 70% during 2017, the signals are normalized by using signals from tiles at $i\eta = 18$ in layer 7, which are expected to have less than 1% reduction in signal output. Differences between data for $i\phi$s 63 and 65 are outside the indicated statistical uncertainties. These differences contribute to the systematic uncertainties described below.

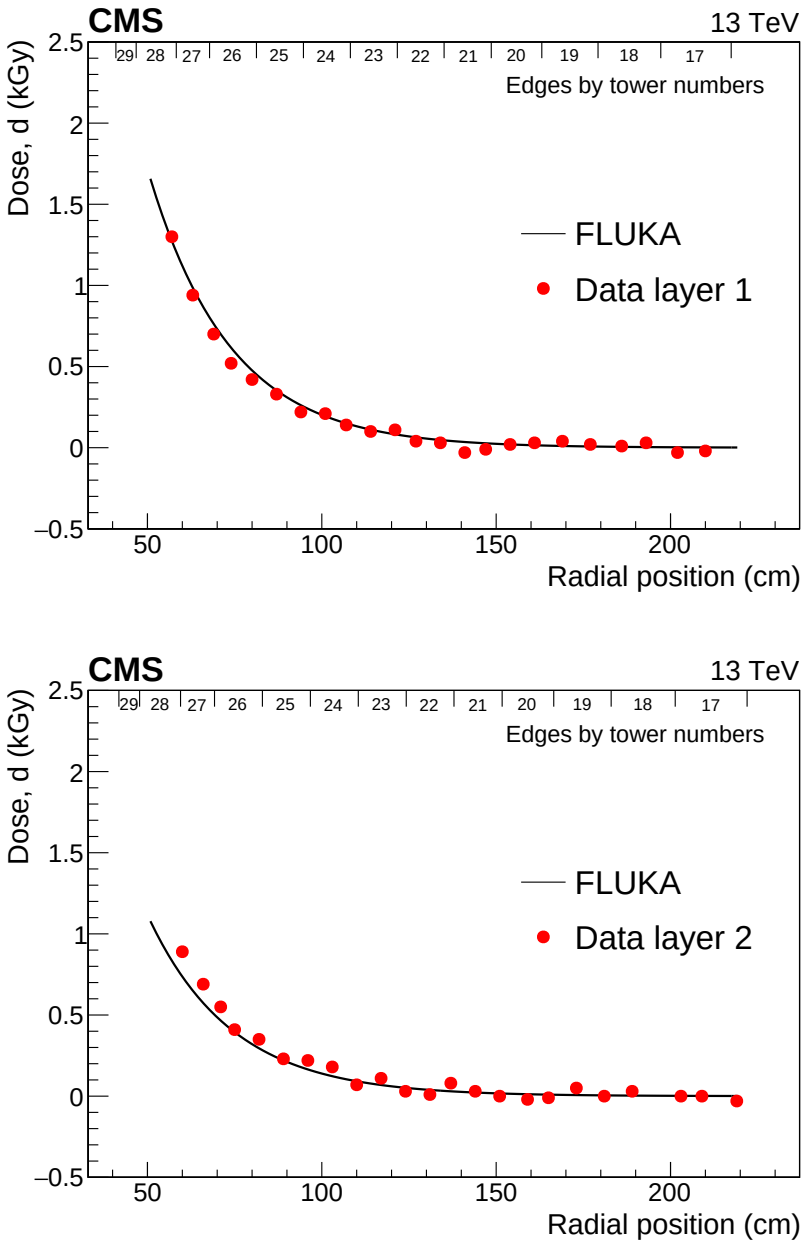

Figure 7: Comparison of doses for the 2015–2016 data-taking periods calculated using FLUKA and measured from dosimeter films in layer 1 (upper) and layer 2 (lower), as a function of radial distance from the beam. Positions of the tile edges in the radial direction are indicated along the tops of the figures.

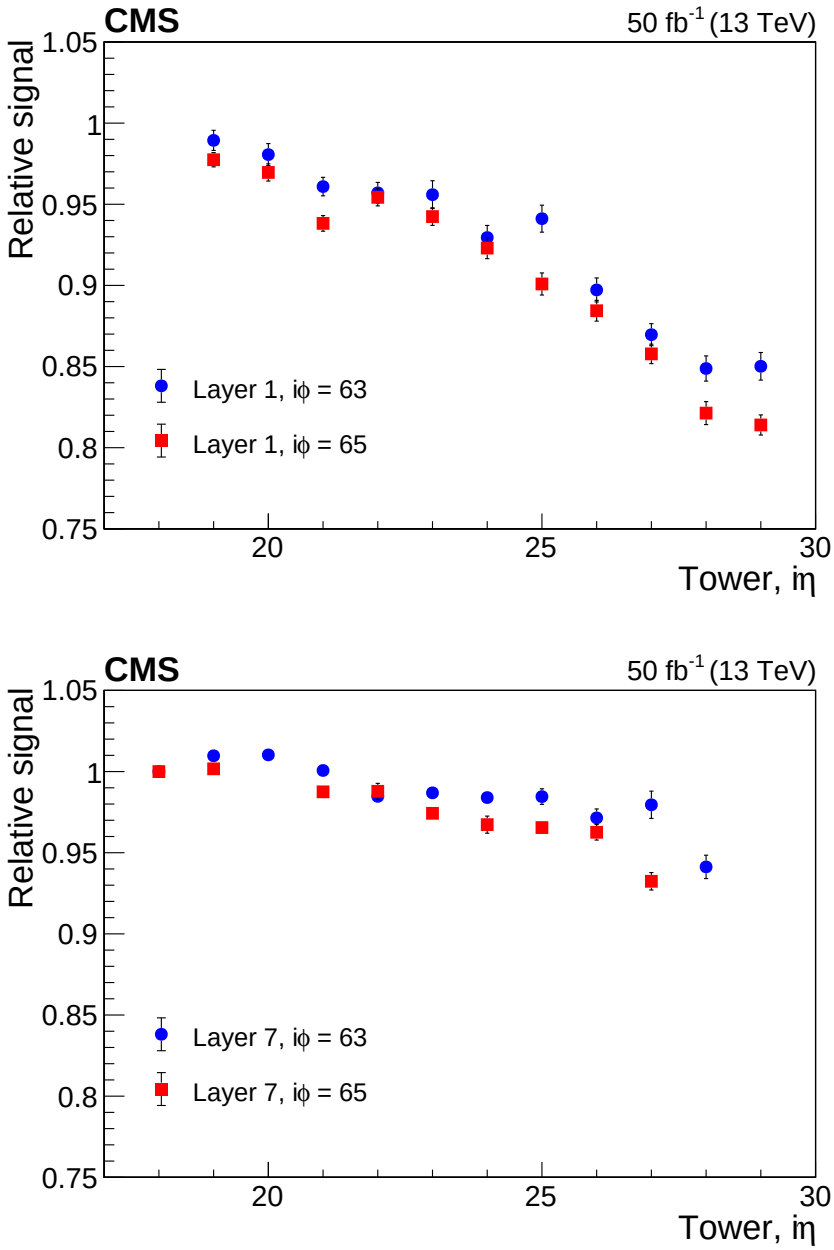

Figure 8: Signal at the end of the 2017 data-taking period from the HE SiPMs, relative to that at the start, as measured using the laser calibration system versus $i\eta$ for SCSN−81 tiles in layer 1 (upper) and layer 7 (lower). Only unscaled statistical uncertainties are shown. The differences between results for the two $i\phi$s indicates unknown systematic uncertainty.

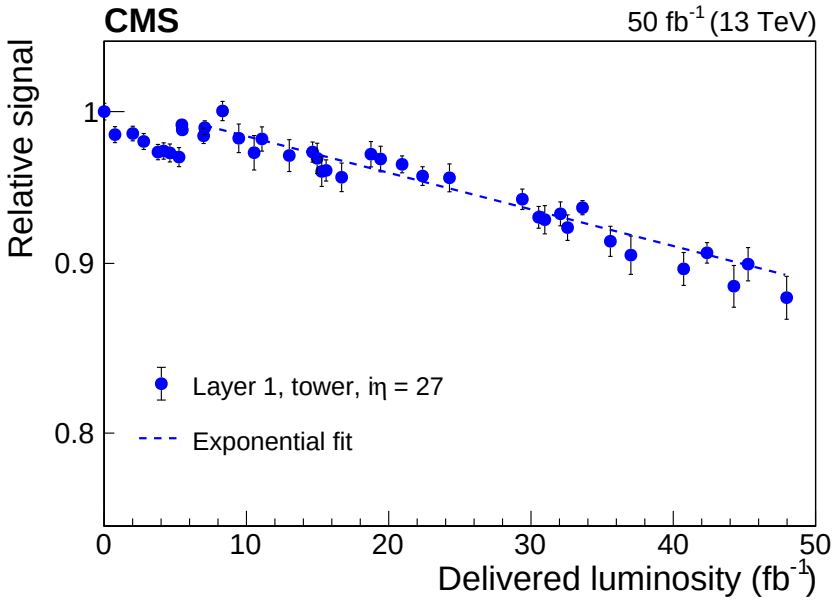

Figure 9: Relative signal measured using the laser calibration system versus delivered luminosity for the SCSN−81 tile in layer 1 with $i\eta = 27$ and $i\phi = 63$. Scaled statistical uncertainties are shown (see text). For this tile, the estimated dose at the end of data taking was $d = 1.5\,\text{kGy}$, and the average dose rate was $R = 0.89\,\text{Gy/h}$. The dashed line represents a fit to the data to obtain the value of the exponential slope. Note that the vertical scale is logarithmic (base 10).

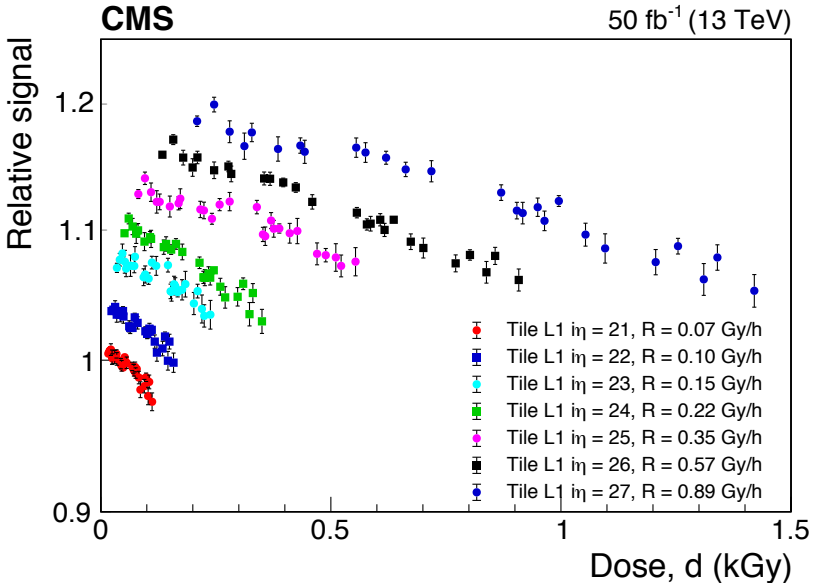

Figure 10: Relative signal for laser light versus accumulated dose for the SCSN−81 tiles in layer 1 with $i\eta = 21$–27. The average dose rates are shown for each set of points. The vertical scale is logarithmic and subsequent sets are shifted up by a factor of 1.03 relative to the previous set for better visibility. Each set starts at the dose corresponding to integrated luminosity of $7\,\text{fb}^{-1}$. Scaled statistical uncertainties are shown (see text).

The normalized signals from individual channels exhibit an approximately exponential decrease versus integrated luminosity over most of the data-taking period. To characterize the behavior of signal loss, we fit the exponential portions of the normalized signal outputs with an exponential function of integrated luminosity, as illustrated in Fig. 9 for one particular tile. A deviation from the expected exponential behavior is observed during the first 7 fb^{-1} of data taking. The reason for this effect is not yet understood and this part of the data is not used in the analysis. With higher luminosity the effects are clearer so we concentrate on this part of the data. The statistical uncertainty in the measured mean signal within a single laser run is smaller than the spread observed when comparing different laser runs taken at similar integrated luminosities. In consequence, fluctuations are observed that are larger than expected based on uncertainties in the mean signal in a single laser run, indicating the presence of an additional source of scatter. We account for these fluctuations by scaling the uncertainties in individual laser points to yield a χ^2 per degree of freedom (dof) of one for the exponential fits. This conservative procedure results in larger estimates of uncertainties in the fit parameters.

Figure 10 presents relative signals versus dose for tiles with $i\eta = 21$–27 in layer 1. The signals show an exponential decrease (as in Eq. 1) during periods of stable luminosity, with slopes that depend on corresponding dose rates. These results imply that at a fixed dose the damage to the scintillators increases with decreasing dose rate, within the range of our measurement.

The values of slopes μ, obtained from the exponential fits, are averaged in bins of R, and converted to $D(R) = 1/\langle\mu\rangle$ for comparisons with other measurements of D. Averaging of μ in bins of dose rate helps to reduce the statistical uncertainties and extends the range of the measurements to lower values of R, especially in the case of source measurements discussed in Section 4.3. The results for $\langle\mu\rangle$ are discussed in Sec. 4.4 and indicate a dose-rate dependence. A similar dose-rate dependence is also observed without averaging of μ in bins of dose rate, but with larger uncertainties in individual points.

We present results for values of R above 0.01 Gy/h. The fractional uncertainties in μ (or D) are large for tiles with little damage. The region $R > 0.1$ Gy/h is well measured with observed signal losses $>$3%.

Various systematic effects have been evaluated. In addition to the differences between signals from different $i\phi$s, we evaluated sensitivities to the variation of the $i\eta$ choice for normalization, the data range used for fitting slopes, and the QIE gain setting. Combining these contributions, the overall systematic uncertainty in μ is estimated to be about 25%. The measurements are not corrected for the varying sizes of the tiles (see the discussion in Section 5).

4.3 Results using the radioactive source

Each individual tile in the HCAL is designed to be serviced by a movable ^{60}Co radioactive source using small tubes, which are integrated into the calorimeter. The ^{60}Co source provides photons with energies of 1.17 and 1.33 MeV. The source is attached to a wire that guides it through the tubes. All tiles except those in layers 0 and 5, whose tubes have obstructions, can be accessed. The source moves at approximately 6 cm/s, and the signal is integrated for 0.1 s for each measurement. The resulting signal is used to monitor the stability of every tile in the HCAL, not just those in layers 1 and 7. The source data analyzed in this paper were collected during the periods when the LHC did not operate, both before the 2017 and 2018 data-taking periods.

The signal strength when the source was far away from a tile is used to estimate the background. The measurements of signal output before the 2018 data-taking period are corrected

(divided by 0.886) for the decay of the source since the previous measurements were made before taking data in 2017. The ratio of the signal obtained before the 2018 data-taking period to that obtained before the 2017 data-taking period measures the attenuation of the signal output due to radiation damage during collisions in 2017, including any post-irradiation annealing effects. No additional normalization of signal ratios versus $i\eta$ is required. Values of the ratio averaged over $i\phi$ as a function of scintillating tile layer number and tower index $i\eta$ are shown in Fig. 11. The signal loss is small for tiles at large radial distance from the beam and for layers that are deeper in the calorimeter.

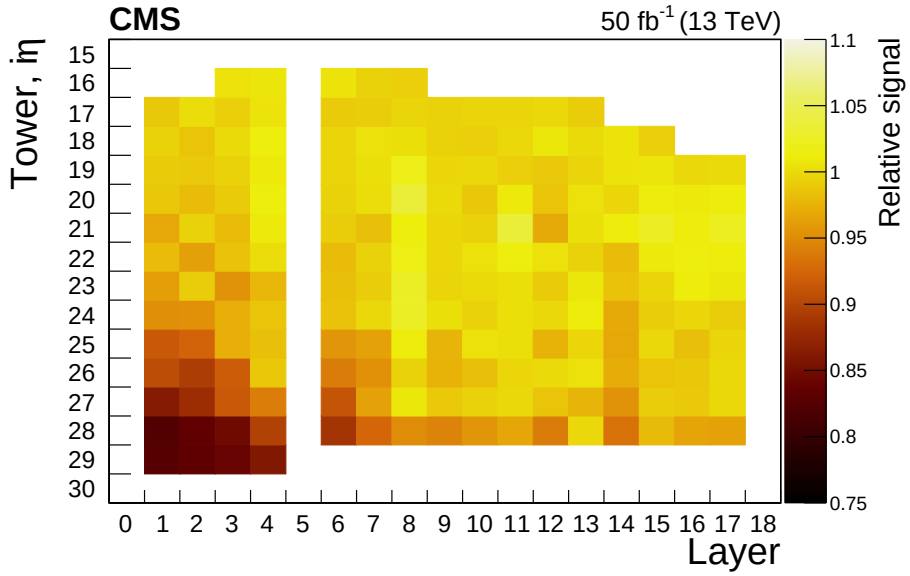

Figure 11: Ratio of ^{60}Co source signals observed before and after the 2017 data-taking period, as a function of $i\eta$ and layer number of scintillator tiles (SCSN−81) in the HE. Tubes in layers 0 and 5 have obstructions and cannot be accessed.

At low R, measurements of signals from individual tiles scatter widely compared to the expected signal loss, due to the size of the measurement uncertainties. However, given the large number of tiles measured, a determination of signal loss can be made even at small values of R assuming that the fluctuations are uncorrelated. The calculated μ values are averaged in bins of R and are displayed in Fig. 12. The uncertainties in $\langle\mu\rangle$ related to the reproducibility of the measurements are included by increasing the statistical uncertainties by a factor 1.4, which results in the average scatter of points around the fit being consistent with the scaled uncertainties. The $\langle\mu\rangle$ values are somewhat lower than, but generally similar to, those from the laser calibration. The source data represent the damage integrated over the entire 2017 data-taking period and include an extended annealing time after the data taking ended. The analyzed laser data exclude the first 7 fb^{-1} and any annealing effects after the end of data taking.

4.4 Parametrization of laser and source results

Figure 12 summarizes the laser and source $\langle\mu\rangle$ results for the SCSN−81 tiles. The data are consistent with a power law dependence of $\langle\mu\rangle$ on R:

$$\langle\mu\rangle = 1/(\alpha\,\rho^{\beta}), \tag{2}$$

where $\rho = R/R_0$, and the constant R_0 can be chosen to minimize the correlation between parameters α and β; the fitted value of α depends on the choice of R_0. This form is equivalent to $D = \alpha\,\rho^{\beta}$. The value of $R_0 = 0.32$ Gy/h is chosen for the fits below so that the correlation

between parameters α and β becomes negligible. The dashed line shown in Fig. 12 is the result of a power-law fit to both sets of data assuming all uncertainties are uncorrelated. The corresponding model parameters are $\alpha = 7.5 \pm 0.3\,\text{kGy}$ and $\beta = 0.35 \pm 0.03$ when $\langle\mu\rangle$ is in kGy^{-1} and R is in units of Gy/h. The fit χ^2/dof is 1.2. A fit to the laser data alone yields $\alpha = 7.3 \pm 0.3\,\text{kGy}$ and $\beta = 0.43 \pm 0.04$, with a χ^2/dof of 0.4. A fit to source data alone gives $\alpha = 7.6 \pm 0.5\,\text{kGy}$ and $\beta = 0.21 \pm 0.06$, with a χ^2/dof of 1.1. The fit to the laser data is inconsistent with no dose-rate effect. The fit to the source data by itself shows a smaller dose-rate effect, and is inconsistent with no dose-rate effect at the 3.5 standard deviation level. For the parameter β, which measures the dose-rate dependence, the difference between the results from the laser and source fits is 0.22 ± 0.08 (2.7 standard deviation). The tension between laser and source results may be a fluctuation. Since the $\langle\mu\rangle$ values from the source data tend to be lower than those from the laser data, additional annealing between the end of pp collisions and the source scan is a possibility. Annealing reduces damage and therefore decreases μ. A future source measurement of the HE and a measurement of annealing effects using post data-taking laser runs would help to reduce this uncertainty.

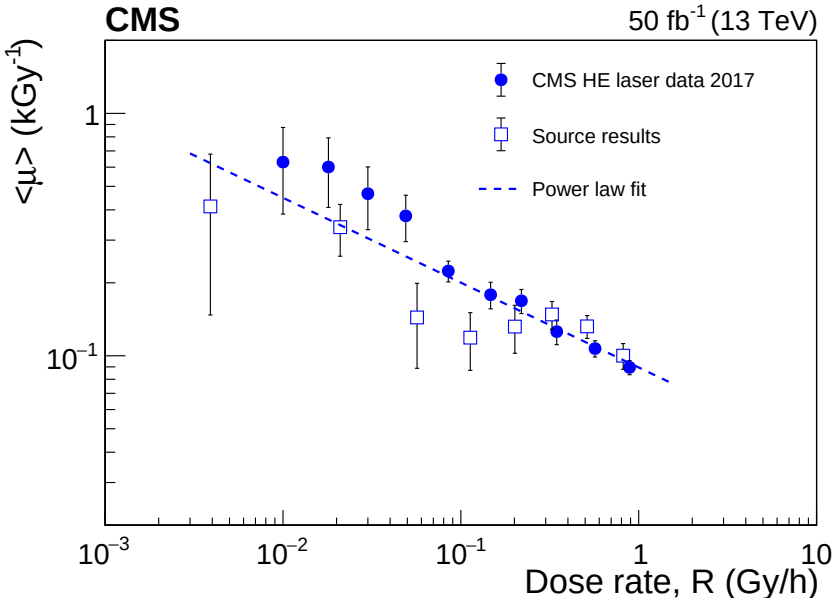

Figure 12: The value of $\langle\mu\rangle$ for SCSN$-$81 tiles as a function of R for laser and source data, parametrized by a power-law behavior, which is shown as a dashed line. The error bars are dominated by systematic uncertainties.

The systematic uncertainty in parameter α is assumed to be the same as the 25% systematic uncertainty in μ, discussed in Sec. 4.2, assuming a 100% correlation between the measurements. For the parameter β, the spread of fit results between the laser and source data indicates systematic effects of the order of 0.1, when varying the range in R used in the fit.

The parametrization of our results should be used with care. It is valid for the decrease in signal output for a system consisting of scintillators, wavelength shifting fibers, and clear fibers made from the same materials we used, and constructed in the CMS tile geometry, when irradiated in the environment of the CMS collision hall. Kuraray has indicated that the current Y$-$11 fiber is not the same as past versions. The parameter values are not generally applicable for other scintillator systems. Extrapolation of the power law above a dose rate of $\approx$10 Gy/h is not expected to be valid. As discussed in Sec. 6, at R of approximately 10 Gy/h, oxygen will no longer permeate the entire tile [13, 29]. Radical creation and termination is different in regions with and without oxygen.

4.5 Cross-checks with inclusive hadrons

An additional method of measuring the effects of irradiation on the tiles is based on the 2017 collision data. Radiation damage is studied using observed energy depositions from hadrons produced in pp collisions. The energy distribution is measured for 25 subsamples distributed uniformly in delivered luminosity over the entire 2017 data-taking period. For each data-taking period n, the ratio of average energy relative to that of period 1,

$$F_{\text{meas}}(n) = \frac{E_{\text{ave}}(n)}{E_{\text{ave}}(1)}, \tag{3}$$

serves as a measure of the radiation damage, where E_{ave} is the average signal measured in all readout channels with the same values of $i\eta$ and depth; the average is calculated from the sum of signals above the threshold of $E_{\text{min}} = 0.5\,\text{GeV}$.

The energy comparison requires a selection of events that is both independent of the HCAL and selects a well-defined set of hard interactions that is stable throughout the period under study. This is fulfilled by utilizing events satisfying a dimuon trigger. The energy ratio is studied as a function of the average number of interactions per bunch crossing, n_{PU}, to take into account the difference in the pileup structure between the periods. The number n_{PU} is estimated from the instantaneous luminosity.

For each value of $i\eta$ and depth, the pileup dependence of F_{meas} is eliminated by fitting it versus n_{PU} with a linear function. The fits are performed in the range $20 < n_{\text{PU}} < 50$ and the values of F_{meas} are extracted at $n_{\text{PU}} = 35$.

The ratio $F_{\text{meas}}(n)$ at $n_{\text{PU}} = 35$ is observed to depend on the energy threshold E_{min}. Both the numerator and denominator of $F_{\text{meas}}(n)$ are sums of energies of those individual channels that are above the threshold E_{min}. In the presence of radiation damage the ratio $F_{\text{meas}}(n)$ will typically be smaller than the ratio $F(n)$ that would be obtained were the threshold not present. The higher the E_{min} threshold, the larger the discrepancy. To correct for this, a calibration is performed as follows. Using data from the first subsample, we multiply the energies contributing to the numerator by scale factors that represent hypothetical signal losses due to radiation damage, but we leave the denominator unchanged.

The values of the scale factors are varied in the range observed in the data, and for each scale factor F' a value F'_{meas} is extracted using the method described above. A linear relationship between F' and F'_{meas} is found, which is used to correct the measured values of $F_{\text{meas}}(n)$ to obtain the corresponding $F(n)$. The magnitude of this correction depends on $i\eta$ and depth, and typically amounts to no more than 20% of the measured signal loss fraction $(1 - F_{\text{meas}}(n))$.

The corrected signal fractions F measured for the channels in the first three depths of $i\eta = 27$ are shown in Fig. 13 (upper), as a function of delivered luminosity. The error bars include a systematic uncertainty of <1%, which results in fit χ^2/dof of around one. A decrease of F with delivered luminosity is clearly seen. A small shift of points near $20\,\text{fb}^{-1}$ is believed to be due to residual luminosity calibration uncertainty during this period. Figure 13 (lower) presents the values of F averaged over $i\phi$ as a function of $i\eta$ and depth after $50\,\text{fb}^{-1}$, showing a decrease of F with increasing $i\eta$ and decreasing depth. The behavior is consistent with that shown for individual tiles observed by the moving source for all the tiles of the HE, albeit with an increased granularity due to a readout in depths and not layers.

Depth 1 consists of a single layer (layer 0) and thus its tiles have well-defined doses and dose rates. Using the same procedure as for the laser data, these data can therefore be converted to $\langle\mu\rangle$ versus R. The results are shown in Fig. 14. The parameters of the power-law fit are

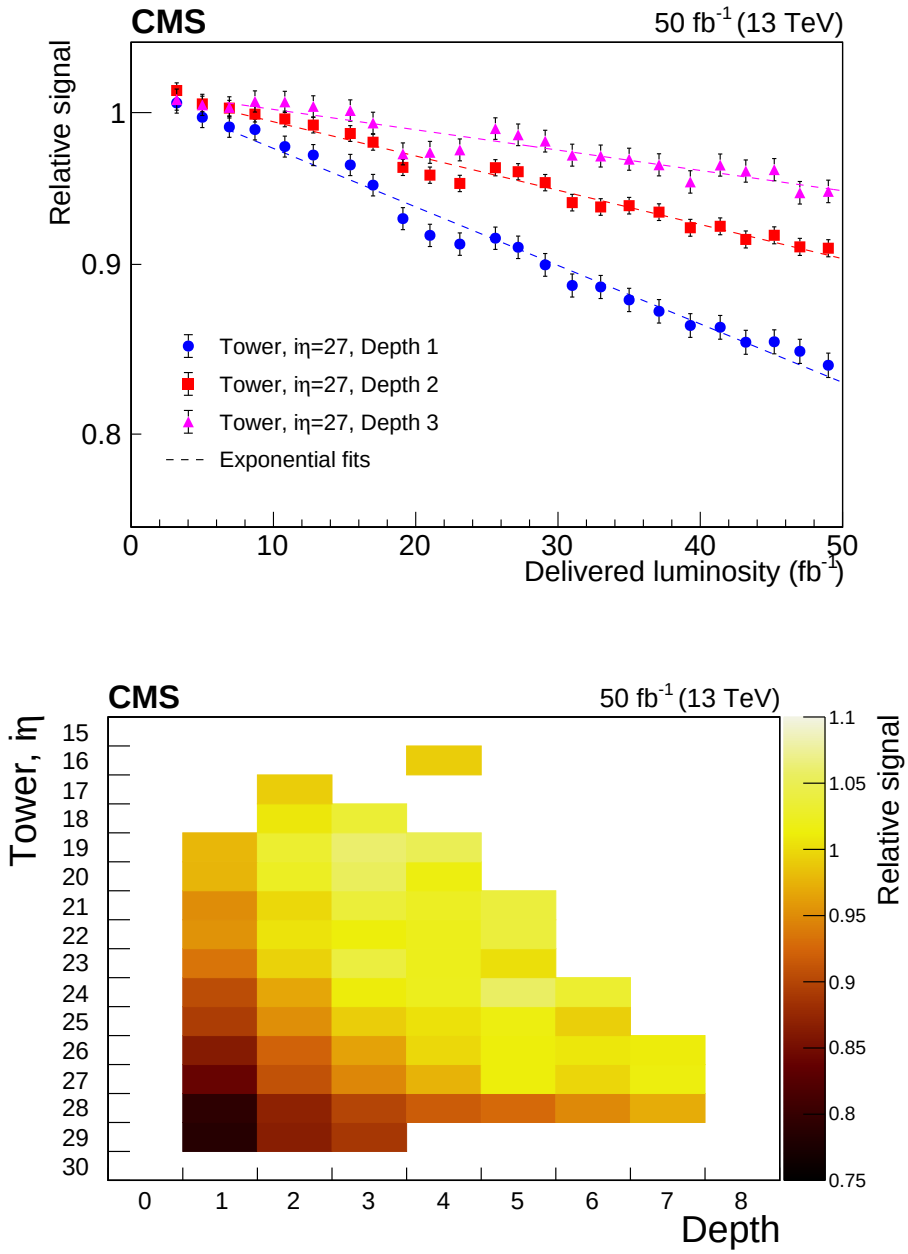

Figure 13: Upper: Relative signal F for $i\eta = 27$ in depths 1, 2, and 3 versus delivered luminosity using the in situ "inclusive" method; the dashed lines show the results of fits with an exponential function, after excluding the first 7 fb^{-1} of data, as was done in the laser data analysis (Sec. 4.2). For the tile in depth 1 (i.e., layer 0), the estimated dose at the end of data taking was $d = 1.5\,\text{kGy}$ and the average dose rate was $R = 0.89\,\text{Gy/h}$. Lower: Relative signal F for towers with $i\eta = 16$–29 at different depths measured after 50 fb^{-1} of delivered luminosity; only results with a relative uncertainty of 3% or lower on measured values of F are shown. Tiles in depth 1 are made of BC−408 and tiles in other depths are SCSN−81.

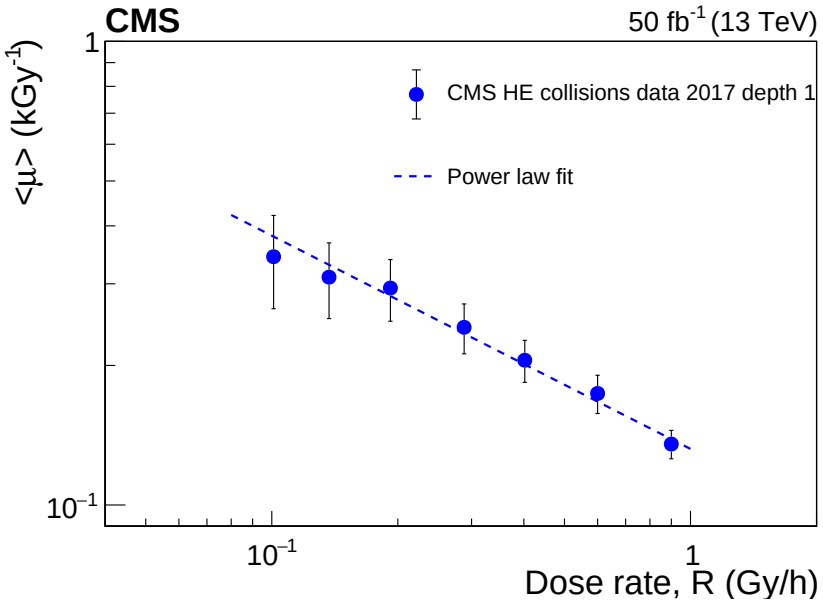

Figure 14: The value of $\langle\mu\rangle$ as a function of R for in situ collision data in depth 1 (BC−408), parametrized by a power law behavior, which is shown as a dashed line.

$\alpha = 5.4 \pm 0.1$ kGy and $\beta = 0.46 \pm 0.04$, with a χ^2/dof of 0.5, for $R_0 = 0.48$ Gy/h. The fit to the layer 0 in situ data is inconsistent with no dose-rate effect. The layer 0 tiles are constructed from PVT instead of PS, and hence their behavior can differ from that of PS-based tiles previously discussed. Nonetheless, the value of β, which parametrizes the dose-rate dependence, is similar to that from the laser measurements. At a given dose rate, the values of $\langle\mu\rangle$ are larger (and the value of the α parameter is smaller) for this PVT-based material, indicating more damage than for the PS-based tiles.

4.6 Cross-checks using isolated muons

The most probable energy deposition by a muon can also be used to estimate the amount of radiation damage. The acceptance of the tracker and of the muon system limits this measurement to portions of the HE where the damage is measured to be small.

The trajectories of forward isolated muon candidates with $p_T > 20$ GeV are propagated to the calorimeter surface to determine which tower they will traverse. The data-taking period is divided into subsamples. For each, a Landau distribution convolved with a Gaussian resolution function is fitted to the charge distribution from the tower to obtain the most probable value (MPV) of deposited charge. A typical spectrum, including the fit, is shown in Fig. 15.

Because of pileup contributions to the measured signal, the isolated muon analysis uses events with a similar number of reconstructed vertices (the range 20–25 was used). The ratio of the MPV plotted as a function of delivered luminosity to that of the first subsample for $i\eta = 26$ depth 1 is shown in Fig. 16.

Only the towers at shallow depths and large $i\eta$ values are damaged sufficiently to detect the losses due to radiation damage in 2017 using this technique. Currently, this measurement is not competitive with other results for these towers. Upgrades for the CMS detector planned for future operations will have a tracking system with a larger η acceptance, extending the usefulness of this technique. Monitoring of calorimeter signals with muons has been tried for the first time using the 2017 data. It is important to develop this technique further for use in

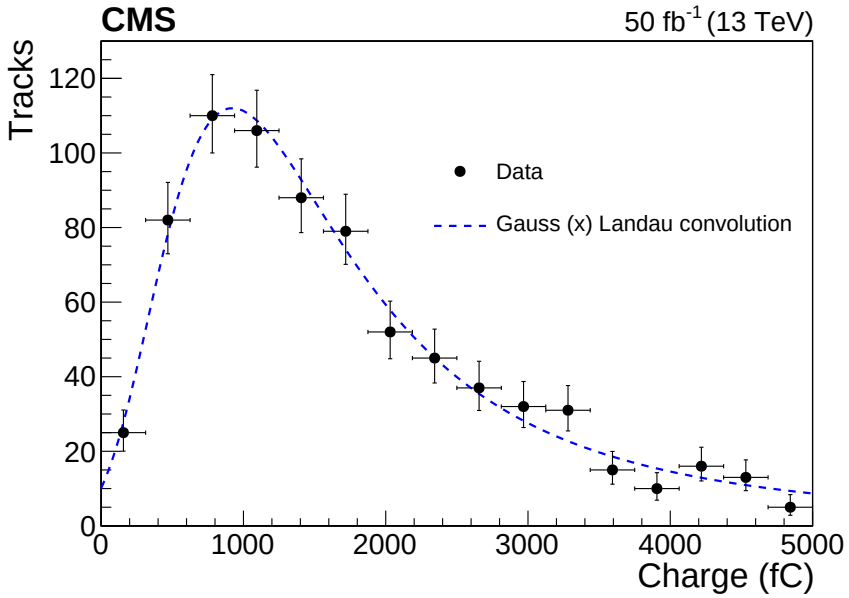

Figure 15: Fit to the charge distribution in an HE tower $i\eta = 26$ depth 1 (BC−408) due to an isolated muon from one of the event samples of 2017 data.

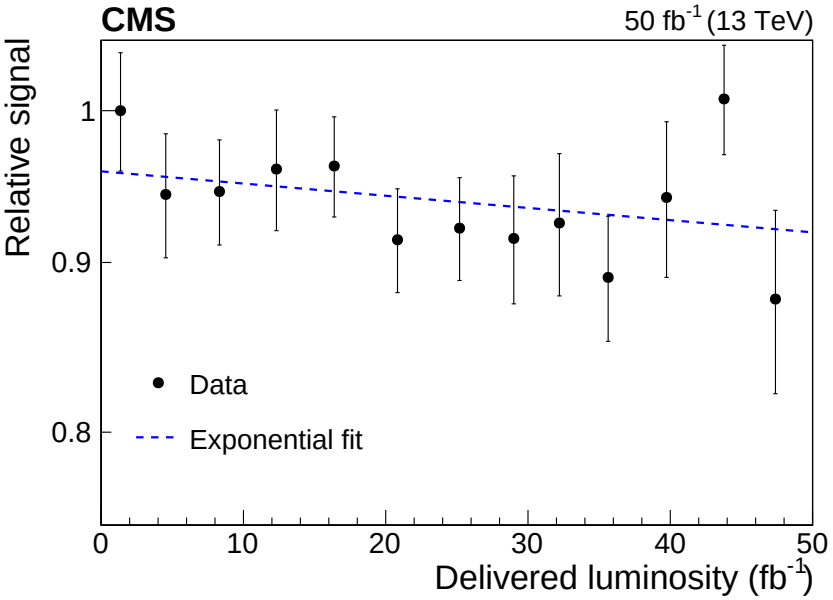

Figure 16: Relative muon signal in an HE tower with $i\eta = 26$ and depth 1 (BC−408) versus delivered luminosity. The dashed line shown on the figure is the result of a fit to an exponential distribution.

future operation.

5 High-dose-rate results using sources

The CMS laser data monitor the HE tile performance for R only up to about 2 Gy/h (see Fig. 12). Intense radioactive sources are used to irradiate plastic scintillator tiles and obtain data at higher R, up to 1 kGy/h. To look at R-dependent effects and to avoid bias from other factors, such as tile geometry or chemical composition, only results from 10 cm $\times$ 10 cm $\times$ 0.37 cm SCSN$-$81 scintillator tiles read out with WLS fibers are reported here, unless noted otherwise. Although temporary damage is small for tiles irradiated in the HE, it is larger at the R values above 100 Gy/h. The values reported in this section reflect the permanent damage to the scintillator tiles remaining after annealing. This was ensured through observation of the signal output versus time.

Some of the data were taken at facilities with ^{60}Co gamma sources, located at the Kharkov Institute of Physics and Technology (KIPT), National Research Nuclear University MEPhI, Goddard Space Flight Center, Argonne National Laboratory (ANL), the Michigan Memorial Phoenix Project, the National Institute of Standards and Technology in Gaithersburg MD, and at the University of Maryland (UMD). We also include a measurement from irradiation using an electron beam at Florida State University (FSU), described in Ref. [30]. For these measurements, some tiles had a fiber with a slightly smaller diameter, and a more recent formulation of Y$-$11 fiber from Kuraray than that used for the HE construction. The machining of the grooves in the tiles was also performed by different machinists using different toolings, and different machining rates. The temperatures of the tiles during the various irradiations are not known precisely, hence the processes affecting the annealing of radicals may differ somewhat.

For the source measurements, the signal output of the samples was measured before and after irradiation to calculate $D(R)$. The exact methods differ from study to study, but the general procedure involves the excitation of the irradiated scintillator tile by particles (e.g., cosmic rays, or alpha or gamma particles from a small, calibrated source placed in contact with the scintillator), and the measurement of the signal output from the WLS fiber via either a photomultiplier tube or a SiPM.

The remainder of the data were taken from samples irradiated in a region forward of CMS called the CASTOR radiation facility (CRF). These tiles were irradiated by particles originating from pp collisions during the 2016 data-taking period. They were located at radial distances from the beam line ranging from 11.8 to 25.9 cm. The doses received by the CRF tiles in 2016 were determined based on film dosimetry measurements and range from 15 to 60 kGy. An additional CRF-based measurement was performed during 2017, using tiles at the radial distance from the beam of 43.2 cm, which received a dose of about 2.3 kGy.

For the CRF measurements, a laser calibration system was used to monitor the signal output of the tiles during the data taking. As shown in Fig. 17, the signal loss as a function of received dose appears to be more rapid in the initial stage of irradiation. The tiles were remeasured in the laboratory after the CRF irradiation. The results of these measurements indicate that the initial drop seen in Fig. 17 was caused by instrumental effects and not radiation damage. The signal output follows an exponential decay for the remainder of the exposure. There is some annealing after day 44, when the exposure ended. The CRF data shown in Fig. 18 are corrected for the observed annealing. Measurements of the tiles after removal from the CRF and replacement of the irradiated WLS fiber with a new one indicate that about 20% of the damage occured in the fiber. The impact of radiation on reflectivity of Tyvek^{TM} is estimated

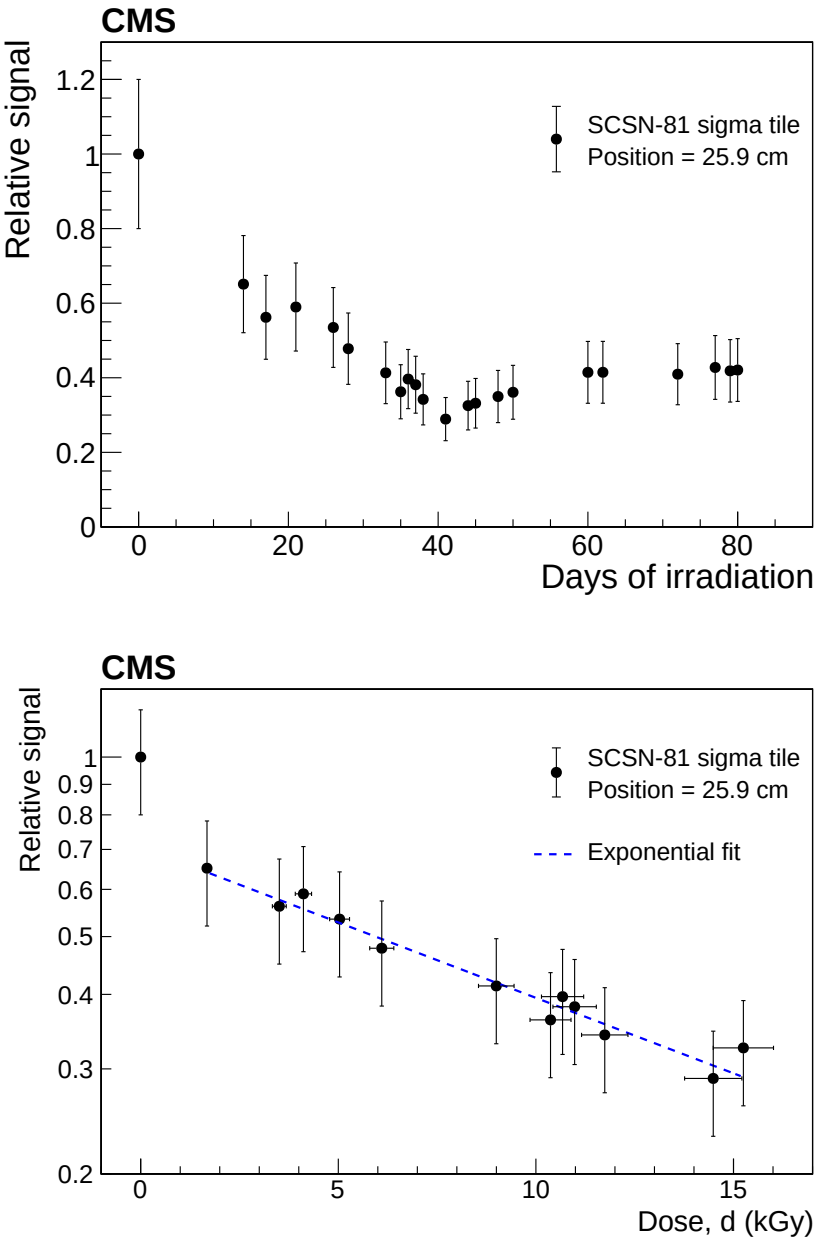

Figure 17: Relative signal for an SCSN−81 tile in the CRF radiation zone, plotted versus time (upper) and versus received dose (lower), for $R = 42\,\mathrm{Gy/h}$.

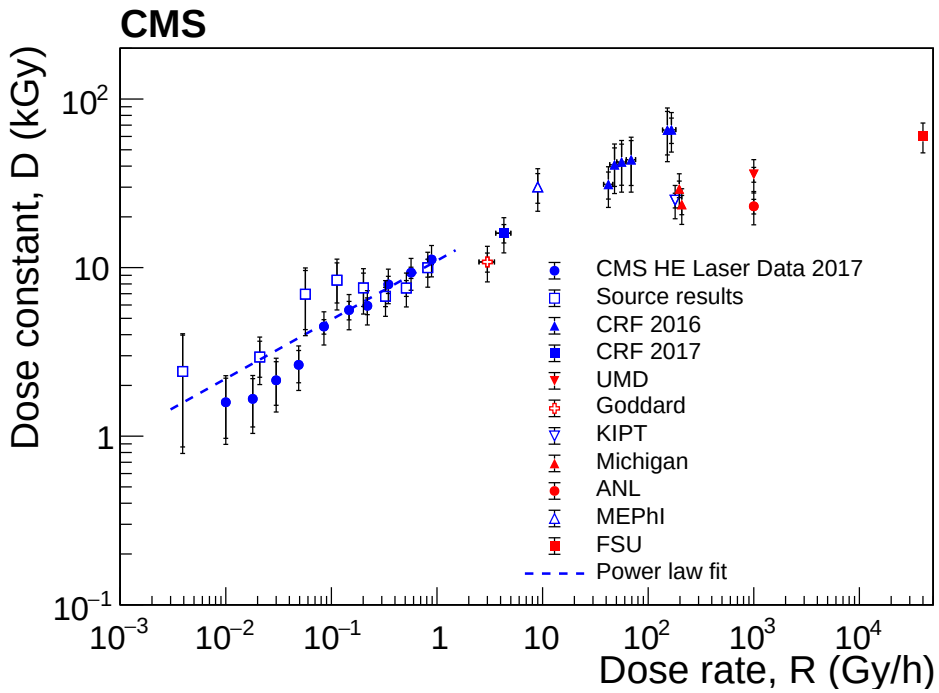

Figure 18: Values of $D(R)$ versus R for high-R data taken with gamma irradiation sources at KIPT, National Research Nuclear University MEPhI, Goddard, Michigan, ANL, and UMD, an electron beam at FSU, and in the collider environment in the CRF for SCSN−81 tiles, along with the results from the HE laser and source calibration data. The statistical uncertainties are shown as the inner bars, and the outer bars include the systematic uncertainties added in quadrature. The error bars on the irradiation data are dominated by systematic uncertainties.

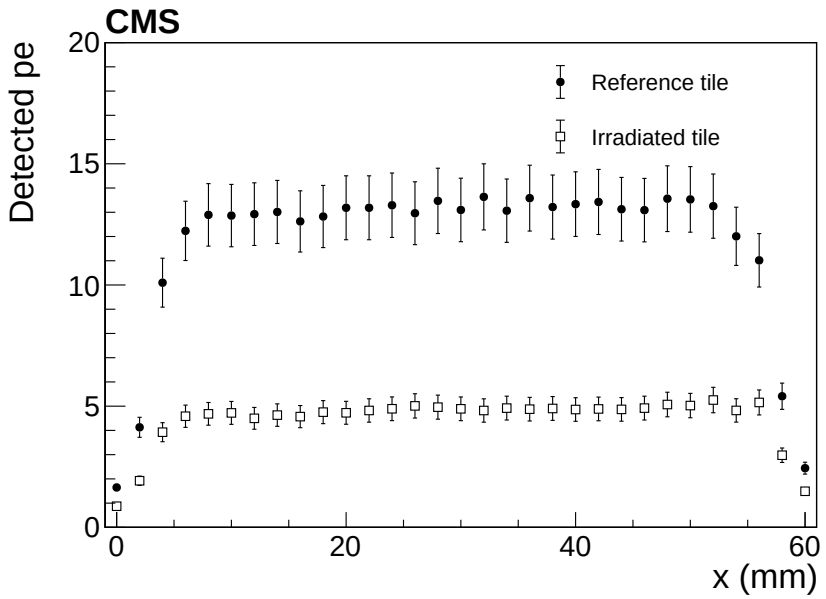

Figure 19: Number of detected photoelectrons for an SCSN−81 tile before and after an irradiation dose of 30 kGy at R of 9 Gy/h, as a function of the position of a radioactive-scan source along an axis through the center of the tile and parallel to one of its sides. The error bars are dominated by systematic uncertainty in normalization of the measurements; statistical point uncertainties are <2%.

by wrapping a single tile in the various Tyvek^{TM} wrappers from the CRF samples exposed to different doses. The light output of such sets was seen to decrease by about 0.2% per 1 kGy of the dose to the Tyvek^{TM} wrappers. We conclude that the impact of Tyvek^{TM} damage on the measurements of light output of the HE channels was negligible.

Figure 18 summarizes the results from the CRF and from electron beam and gamma source irradiations, along with the HE laser and source results. We are not aware of other measurements of closely comparable tile-fiber systems at the low dose rates seen by the HE scintillators. For several orders of magnitude in R, $D(R)$ shows an apparent R-dependence. The exact causes and mechanisms behind this effect remain to be understood. In the next section, we compare the observed dependence to what is known about dose-rate effects in plastic scintillators.

Tiles irradiated at gamma sources are also used to investigate the uniformity of the signal output after irradiation and to check the dependence of $D(R)$ on the tile size. A transverse scan of the signal output of a tile that received a total dose of 30 kGy at an R of 9 Gy/h is shown in Fig. 19. The number of photoelectrons (pe) detected in scans prior to irradiation is fairly independent of the source position. The irradiated tile retains its uniformity after absorbing this large dose, implying that it is unlikely that optical light attenuation is the major component of the observed signal loss. Reference [31] came to similar conclusions based on Raman data, albeit for a PVT-based scintillator.

In addition, tiles with a thickness of 0.37 cm and sizes of 20 cm $\times$ 20 cm, 12 cm $\times$ 9 cm, and 5 cm $\times$ 8 cm were irradiated at R of 1 kGy/h with doses of 1, 10, 20, 50, and 100 kGy. The extracted values of D are similar, to within $\pm$20%.

We also investigated light propagation in tiles based on GEANT4 [32] ray tracing. Tile damage is simulated using the measured density of color centers. This study indicates that the effect of tile size is expected to be small (at most 20%).

6 Discussion of dose-rate effects

Because dose-rate effects have a significant impact on the performance of scintillator-based detectors at hadron colliders, in this section we review what is known of their origins. Polymers are complex molecules, and their structure depends on the details of their preparation and the presence of additives such as antioxidants, while their behavior depends in detail on their environment. Therefore, extrapolating from measurements of a specific plastic in a specific environment to another plastic and/or environment is difficult. Measurements of new plastics and new environments will always be necessary. However, existing theory facilitates a deeper understanding of the results of our measurements.

Two well-studied [11, 13, 33–37] sources of dose-rate effects in plastic scintillators are related to oxygen, one involving the diffusion of oxygen into the plastic during irradiation, and the other involving the rate of polymer oxidation in the areas containing oxygen. Polymer oxidation can be either beneficial or detrimental, depending on the dose rate and the details of the plastic preparation, the presence of additives such as antioxidants, and environment. While the magnitude of polymer oxidation depends on such details, theory gives us some guidance as to its dose-rate dependence.

As shown in the diagrams in Fig. 2, different kinds of termination, and thus permanent color centers (see Section 2), are possible when oxygen is present. Oxygen is highly reactive and polymer oxidation occurs quickly after the production of the radicals [11, 13, 33–37]. In this case, there is little of the temporary damage that is indicative of radicals, and little to no annealing.

Since the final products involving oxygen tend to absorb UV light, there can be considerable permanent damage that results in what is called reduction of light output [20] (see Section 2). Temporary damage is larger without oxygen, as there is no oxygen to quickly bind to the radicals. However, as the radicals slowly reform bonds, the resulting stable structures sometimes have a small probability to absorb visible light, reducing the plastic's absorption length. Given the tension between these two competing effects, more experiments are needed to determine the optimum atmosphere for different materials, dose rates, temperatures, and doses. It is challenging to predict the optimal amount of oxygen for a given value of R.

For a given plastic and environment, theory allows some numerical extrapolation between different values of R. At high enough R, the density of radicals produced is high enough that oxygen cannot diffuse into the plastic fast enough to bind to and neutralize all the produced radicals, and thus cannot penetrate beyond a depth that depends on the dose rate [37, 38]. The depth z_0 for oxygen diffusion into the plastic for a rectangular slab of plastic is [37]

$$z_0^2 = \frac{2\,M\,C_0}{\mathrm{Y}\,R} = \frac{2\,M\,S\,P}{\mathrm{Y}\,R}, \tag{4}$$

where M is the diffusion coefficient for oxygen, C_0 is the oxygen concentration on its edge, Y is the specific rate constant of active site formation, S is the oxygen solubility, and P is the external oxygen pressure. There is an abrupt transition between areas with and without oxygen. The oxygen concentration in the oxidized regions is almost uniform [29]. For PS tiles with a thickness of 4 mm, oxygen permeates the entire sample for R below (roughly, depending on the plastic preparation and environment) 10 Gy/h [13, 29]; annealing should be small below this R. For R above this value, polymer oxidation will occur only in the region permeated by oxygen, contributing to an R dependence of the damage to the scintillator.

The second source of dose-rate effects is related to the rate of polymer oxidation in regions with oxygen [33, 36]. The rate of polymer oxidation is [33, 34, 39]

$$K(C(x,t)) = -\frac{C_1\,C(x,t)}{1 + C_2\,C(x,t)}, \tag{5}$$

where $-K(C(x,t))$ is the rate at which oxygen is bound to the polymer, x is the position relative to the surface of the material where the rate is being measured, and $C(x,t)$ is the concentration of oxygen. The constants C_1 and C_2 depend on the kinematics of the chemical reactions. The constant C_1 is related to polymer oxidation from radicals, while C_2 is related to stable terminations of polymer oxidation. The constant C_1 is proportional to the square root of R for bimolecular reactions (leading to a dose-rate effect) and to R for unimolecular reactions (no dose-rate effect).

Another possible explanation for dose-rate effects involving oxygen for acrylic scintillators (PMMA) is postulated in Ref. [40]. Radiation damage in PMMA is generally larger, for the same dose, than in either PS or PVT. The material produces more radicals and gas per dose than PS or PVT and does not cross link [13]. The authors suggest that oxygen ions, produced by the radiation in the atmosphere surrounding the material, may diffuse into the material and break polymer bonds, and that the damage may be accentuated in the presence of UV light. An irradiation at 0.1 Gy/h showed no damage when the samples were in a nitrogen atmosphere, while damage was clearly seen for air and oxygen atmospheres.

According to Ref. [18], dose-rate effects can also be caused by a change in the relative amount of thermal- and radiation-induced damage. At low R, damage due to thermal effects becomes more important. Because thermal photons are of lower energy, they can only break the lowest

energy bonds, changing what types of radicals are formed. This source of dose-rate effects is important when performing aging studies at high temperature.

Other possible sources of dose-rate effects include damage to the fluors [13], damage to the fiber, presence of ozone [41], and an unknown mechanism observed in PS at high R that is present at 22° C but not at 60° C [29].

Because dose-rate effects are seen in the HE tiles at $R < 10\,\mathrm{Gy/h}$ when oxygen fully permeates the plastic, the cause cannot be its penetration depth (see Eq. 4), even though the power dependence close to 0.5 is suggestive. The power dependence is in between that expected for unimolecular and bimolecular terminations of radicals (see Eq. 5) [11, 13, 33–37]. There is a suggestion of a change of slope at a dose rate of 10 Gy/h, which, if real, could be caused by different chemical processes in the regions with and without oxygen above this dose rate.

7 Summary and conclusions

Radiation damage due to particles produced in pp collisions at $\sqrt{s} = 13\,\mathrm{TeV}$ in two types of plastic scintillator tiles in the CMS hadron endcap calorimeter has been studied using data from several sources: a laser calibration system, a movable radioactive source, as well as hadrons and muons produced in pp collisions. Within the range of our measurements, the results from the various methods indicate that at a fixed dose the damage to the scintillators increases with decreasing dose rate. The dose-rate dependence is most accurately measured by the laser system, with larger uncertainties in the other measurements. The signal has an exponential decrease with dose characterized by dose constant D, which as a function of dose rate R is compatible with a power law with an exponent of about 0.4 for both PS and PVT-based tiles, in between the values predicted by bimolecular and unimolecular terminations of radicals [11, 13, 33–37]. The PVT-based tiles indicate more damage than the PS-based tiles for the same exposure. For $R \approx 100\,\mathrm{Gy/h}$, approximately 20% of the damage occurs in the fiber. The results are compared to damage produced by irradiations with ^{60}Co sources and by an electron beam. At dose rates less than 10 Gy/h, relevant for future experiments at particle colliders, where oxygen has saturated the plastic, the amount of damage does not depend on the particle type.

The parameters of the power-law fit are functions of the detector geometry, materials, ambient conditions, etc. More studies are required to derive a general parametrization. Nonetheless, fits such as these above have been used to predict the future behavior of the CMS hadron barrel and endcap calorimeters [6, 42].

Several aspects of the data-taking conditions in the CMS detector give rise to systematic uncertainties that are difficult to estimate. A set of identical tile + WLS fiber assemblies subjected to varying dose-rate exposures in a temperature-controlled laboratory, with careful monitoring throughout a year-long exposure, would allow for a large reduction in the systematic uncertainties. At high dose rates, the amount of damage has a considerable spread, possibly indicating underestimated systematic uncertainties, motivating further studies to determine the underlying cause. It would be interesting to have data over this wide range of dose rates separately for the fibers and for the plastic tiles, to see their separate power dependencies. Studies of tiles at low dose rates in an oxygen-free environment, like a nitrogen atmosphere as suggested in Ref. [40], are needed to test directly if the cause is dose-rate dependent polymer oxidation. It would also be helpful to make measurements above 10 Gy/h using a set of tiles made in a uniform way and irradiated at a known temperature.

Dose-rate effects can be large at low dose rates and should be measured for new tile systems.

Acknowledgments

We congratulate our colleagues in the CERN accelerator departments for the excellent performance of the LHC and thank the technical and administrative staffs at CERN and at other CMS institutes for their contributions to the success of the CMS effort. In addition, we gratefully acknowledge the computing centres and personnel of the Worldwide LHC Computing Grid for delivering so effectively the computing infrastructure essential to our analyses. Finally, we acknowledge the enduring support for the construction and operation of the LHC and the CMS detector provided by the following funding agencies: BMBWF and FWF (Austria); FNRS and FWO (Belgium); CNPq, CAPES, FAPERJ, FAPERGS, and FAPESP (Brazil); MES (Bulgaria); CERN; CAS, MoST, and NSFC (China); COLCIENCIAS (Colombia); MSES and CSF (Croatia); RPF (Cyprus); SENESCYT (Ecuador); MoER, ERC IUT, PUT and ERDF (Estonia); Academy of Finland, MEC, and HIP (Finland); CEA and CNRS/IN2P3 (France); BMBF, DFG, and HGF (Germany); GSRT (Greece); NKFIA (Hungary); DAE and DST (India); IPM (Iran); SFI (Ireland); INFN (Italy); MSIP and NRF (Republic of Korea); MES (Latvia); LAS (Lithuania); MOE and UM (Malaysia); BUAP, CINVESTAV, CONACYT, LNS, SEP, and UASLP-FAI (Mexico); MOS (Montenegro); MBIE (New Zealand); PAEC (Pakistan); MSHE and NSC (Poland); FCT (Portugal); JINR (Dubna); MON, RosAtom, RAS, RFBR, and NRC KI (Russia); MESTD (Serbia); SEIDI, CPAN, PCTI, and FEDER (Spain); MOSTR (Sri Lanka); Swiss Funding Agencies (Switzerland); MST (Taipei); ThEPCenter, IPST, STAR, and NSTDA (Thailand); TUBITAK and TAEK (Turkey); NASU (Ukraine); STFC (United Kingdom); DOE and NSF (USA).

Individuals have received support from the Marie-Curie programme and the European Research Council and Horizon 2020 Grant, contract Nos. 675440, 752730, and 765710 (European Union); the Leventis Foundation; the A.P. Sloan Foundation; the Alexander von Humboldt Foundation; the Belgian Federal Science Policy Office; the Fonds pour la Formation à la Recherche dans l'Industrie et dans l'Agriculture (FRIA-Belgium); the Agentschap voor Innovatie door Wetenschap en Technologie (IWT-Belgium); the F.R.S.-FNRS and FWO (Belgium) under the "Excellence of Science – EOS" – be.h project n. 30820817; the Beijing Municipal Science & Technology Commission, No. Z191100007219010; the Ministry of Education, Youth and Sports (MEYS) of the Czech Republic; the Deutsche Forschungsgemeinschaft (DFG) under Germanys Excellence Strategy – EXC 2121 "Quantum Universe" – 390833306; the Lendület ("Momentum") Programme and the János Bolyai Research Scholarship of the Hungarian Academy of Sciences, the New National Excellence Program ÚNKP, the NKFIA research grants 123842, 123959, 124845, 124850, 125105, 128713, 128786, and 129058 (Hungary); the Council of Science and Industrial Research, India; the HOMING PLUS programme of the Foundation for Polish Science, cofinanced from European Union, Regional Development Fund, the Mobility Plus programme of the Ministry of Science and Higher Education, the National Science Center (Poland), contracts Harmonia 2014/14/M/ST2/00428, Opus 2014/13/B/ST2/02543, 2014/15/B/ST2/03998, and 2015/19/B/ST2/02861, Sonata-bis 2012/07/E/ST2/01406; the National Priorities Research Program by Qatar National Research Fund; the Ministry of Science and Education, grant no. 14.W03.31.0026 (Russia); the Programa Estatal de Fomento de la Investigación Científica y Técnica de Excelencia María de Maeztu, grant MDM-2015-0509 and the Programa Severo Ochoa del Principado de Asturias; the Thalis and Aristeia programmes cofinanced by EU-ESF and the Greek NSRF; the Rachadapisek Sompot Fund for Postdoctoral Fellowship, Chulalongkorn University and the Chulalongkorn Academic into Its 2nd Century Project Advancement Project (Thailand); the Kavli Foundation; the Nvidia Corporation; the SuperMicro Corporation; the Welch Foundation, contract C-1845; and the Weston Havens Foundation (USA).

References

[1] C. Zorn, "Plastic and liquid organic scintillators", p. 218. doi:10.1142/9789814360333_0004.

[2] CMS Collaboration, "The CMS experiment at the CERN LHC", *JINST* **3** (2008) S08004, doi:10.1088/1748-0221/3/08/S08004.

[3] CMS Collaboration, "Design, performance, and calibration of CMS hadron-barrel calorimeter wedges", *Euro. Phys. J. C* **55** (2008) 159, doi:10.1140/epjc/s10052-008-0573-y.

[4] CMS Collaboaration, "The CMS hadron calorimeter project", Technical Report CERN-LHCC-97-031, 1997.

[5] L. Evans and P. Bryant (editors), "LHC Machine", *JINST* **3** (2008) S08001, doi:10.1088/1748-0221/3/08/S08001.

[6] CMS Collaboration, "The Phase-2 upgrade of the CMS endcap calorimeter", Technical Report CERN-LHCC-2017-023, 2017.

[7] CMS Collaboration, "Dose-rate effects in the radiation damage of the plastic scintillators of the CMS hadron endcap calorimeter", *JINST* **11** T10004, doi:10.1088/1748-0221/11/10/T10004. [Erratum: doi:10.1088/1748-0221/14/08/E08001].

[8] R. A. Shukla et al., "Microscopic characterisation of photodetectors used in the hadron calorimeter of the Compact Muon Solenoid experiment", *Rev. Sci. Instrum.* **90** (2019) 023303, doi:10.1063/1.5046465.

[9] T. Förster, "Zwischenmolekulare energiewanderung und fluoreszenz", *Ann. Phys. (Berl.)* **437** (1947) 55, doi:10.1002/andp.19484370105.

[10] J. B. Birks, "The theory and practice of scintillation counting". International Series of Monographs on Electronics and Instrumentation, Volume 27. Pergamon Press, The Macmillan Company, New York, 1964. doi:10.1016/C2013-0-01791-4, ISBN 1483123642.

[11] E. Biagtan et al., "Gamma dose and dose-rate effects on scintillator light output", *Nucl. Instrum. Meth. B* **108** (1996) 125, doi:10.1016/0168-583X(95)00874-8.

[12] U. Holm and K. Wick, "Radiation stability of plastic scintillators and wave-length shifters", *IEEE Trans. Nucl. Sci.* **36** (1989) 579, doi:10.1109/23.34504.

[13] K. Wick et al., "Recovery and dose-rate dependence of radiation damage in scintillators, wavelength shifters and light guides", *Nucl. Instrum. Meth. B* **61** (1991) 472, doi:10.1016/0168-583X(91)95325-8.

[14] B. Bicken et al., "Recovery and permanent radiation damage of plastic scintillators at different dose rates", *IEEE Trans. Nucl. Sci.* **38** (1991) 188, doi:10.1109/23.289295.

[15] B. Bicken et al., "Influence of temperature treatment on radiation stability of plastic scintillator and wave-length shifter", *IEEE Trans. Nucl. Sci.* **39** (1992) 1212, doi:10.1109/23.173180.

[16] A. D. Bross and A. Pla-Dalmau, "Radiation damage of plastic scintillators", *IEEE Trans. Nucl. Sci.* **39** (1992) 1199, doi:10.1109/23.173178.

[17] N. D. Giokaris et al., "Study of dose-rate effects on the radiation damage of polymer-based SCSN23, SCSN81, SCSN81+Y7, SCSN81+Y8 and 3HF scintillators", *Radiat. Phys. Chem.* **41** (1993) 315, doi:10.1016/0969-806X(93)90069-7.

[18] K. Gillen and M. Celina, "Predicting polymer degradation and mechanical property changes for combined radiation-thermal aging environments", *Rubber Chemistry & Technology* **91** (2018) 27, doi:10.5254/rct.18.81679.

[19] I. B. Berlman, "The effect of massive ^{60}Co doses on the light output of a scintillator solution", Radiological Physics Division Semiannual Report for July through December 1957 ANL-5829, Argonne National Laboratory, 1958.

[20] R. Clough et al., "Discoloration and subsequent recovery of optical polymers exposed to ionizing radiation", *Poly. Degrad. and Stab.* **49** (1995) 305, doi:10.1016/0141-3910(95)87013-X.

[21] CMS Collaboration, "Description and performance of track and primary-vertex reconstruction with the CMS tracker", *JINST* **9** (2014) P10009, doi:10.1088/1748-0221/9/10/P10009, arXiv:1405.6569.

[22] CMS Collaboration, "The CMS trigger system", *JINST* **12** (2017) P01020, doi:10.1088/1748-0221/12/01/P01020, arXiv:1609.02366.

[23] P. Cushman, A. Heering, and A. Ronzhin, "Custom HPD readout for the CMS HCAL", *Nucl. Instrum. Meth. A* **442** (2000) 289, doi:10.1016/S0168-9002(99)01236-X.

[24] Y. Musienko et al., "Radiation damage studies of silicon photomultipliers for the CMS HCAL Phase-1 upgrade", *Nucl. Instrum. Meth. A* **787** (2015) 319, doi:10.1016/j.nima.2015.01.012.

[25] A. Heering et al., "Parameters of the preproduction series SiPMs for the CMS HCAL Phase-1 upgrade", *Nucl. Instrum. Meth. A* **824** (2016) 115, doi:10.1016/j.nima.2015.11.035.

[26] T. M. Shaw et al., "Front-end readout electronics for the CMS Hadron Calorimeter", in *Proceedings, Nuclear Science Symposium Conference Record, 2002, (IEEE)*, p. 194. 2002. doi:10.1109/NSSMIC.2002.1239297.

[27] A. Ferrari, P. R. Sala, A. Fasso, and J. Ranft, "FLUKA: A multi-particle transport code", (2005). CERN-2005-010, SLAC-R-773, INFN-TC-05-11.

[28] T. T. Bohlen et al., "The FLUKA code: Developments and challenges for high energy and medical applications", *Nucl. Data Sheets* **120** (2014) 211, doi:10.1016/j.nds.2014.07.049.

[29] K. Gillen, J. Wallace, and R. Clough, "Dose-rate dependence of the radiation-induced discoloration of polystyrene", *Radiat. Phys. Chem.* **41** (1993) 101, doi:10.1016/0969-806X(93)90046-W.

[30] V. Hagopian et al., "Single tile-fiber unit of SDC calorimeter", *Radiat. Phys. Chem.* **41** (1993) 401, doi:10.1016/0969-806X(93)90078-9.

[31] H. Jivan et al., "Radiation hardness of plastic scintillators for the tile calorimeter of the ATLAS detector", *J. Phys.: Conf. Series* **645** (2015) 012019, doi:10.1088/1742-6596/645/1/012019.

[32] GEANT4 Collaboration, "GEANT4—a simulation toolkit", *Nucl. Instrum. Meth. A* **506** (2003) 250, doi:10.1016/S0168-9002(03)01368-8.

[33] S. W. Shalaby and R. L. Clough, "Radiation effects on polymers", *Am. Chem. Soc. Symp. Ser.* **475** (1991) 457.

[34] J. L. Bolland, "Kinetic studies in the chemistry of rubber and related materials. I. The thermal oxidation of ethyl linoleate", *J. L. Proc. R. Soc. A* **186** (1946) 218, doi:10.1098/rspa.1946.0040.

[35] J. Bolland, "Kinetic studies in the chemistry of rubber and related materials. VII.—influence of chemical structure on the α-methylenic reactivity of olefins", *Trans. Faraday Soc.* **46** (1950) 358, doi:10.1039/TF9504600358.

[36] L. Q. Bateman, "Olefin oxidation", *Q. Rev. Chem. Soc* **8** (1954) 147, doi:10.1039/QR9540800147.

[37] A. V. Cunliffe and A. Davis, "Photo-oxidation of thick polymer samples — Part II: The influence of oxygen diffusion on the natural and artificial weathering of polyolefins", *Polym. Degrad. Stab.* **4** (1982) 17, doi:10.1016/0141-3910(82)90003-9.

[38] T. Seguchi et al., "Radiation induced oxidative degradation of polymers—I: Oxidation region in polymer films irradiated in oxygen under pressure", *Radiat. Phys. Chem.* **17** (1981) 195, doi:10.1016/0146-5724(81)90331-9.

[39] K. Gillen and R. Clough, "Rigorous experimental confirmation of a theoretical model for diffusion-limited oxidation", *Polymer* **38** (1992) 1929, doi:10.1016/0032-3861(92)90280-A.

[40] Y. Sirois and R. Wigmans, "Effects of long-term low-level exposure to radiation as observed in acrylic scintillator", *Nucl. Instrum. Meth. A* **240** (1985) 262, doi:10.1016/0168-9002(85)90634-5.

[41] R. Clough and K. Gillen, "Polymer degradation under ionizing radiation: The role of ozone", *J. Polym. Sci. A: Polymer Chemistry* **27** (1989) 2313, doi:10.1002/pola.1989.080270715.

[42] CMS Collaboration, "The Phase-2 upgrade of the CMS barrel calorimeters", Technical Report CERN-LHCC-2017-011, 2017.

A The CMS Collaboration

Yerevan Physics Institute, Yerevan, Armenia
A.M. Sirunyan[†], A. Tumasyan

Institut für Hochenergiephysik, Wien, Austria
W. Adam, F. Ambrogi, T. Bergauer, J. Brandstetter, M. Dragicevic, J. Erö, A. Escalante Del Valle, M. Flechl, R. Frühwirth[1], M. Jeitler[1], N. Krammer, I. Krätschmer, D. Liko, T. Madlener, I. Mikulec, N. Rad, J. Schieck[1], R. Schöfbeck, M. Spanring, D. Spitzbart, W. Waltenberger, C.-E. Wulz[1], M. Zarucki

Institute for Nuclear Problems, Minsk, Belarus
V. Chekhovsky, M. Korzhik, A. Litomin

Universiteit Antwerpen, Antwerpen, Belgium
M.R. Darwish, E.A. De Wolf, D. Di Croce, X. Janssen, A. Lelek, M. Pieters, H. Rejeb Sfar, H. Van Haevermaet, P. Van Mechelen, S. Van Putte, N. Van Remortel

Vrije Universiteit Brussel, Brussel, Belgium
F. Blekman, E.S. Bols, S.S. Chhibra, J. D'Hondt, J. De Clercq, D. Lontkovskyi, S. Lowette, I. Marchesini, S. Moortgat, Q. Python, K. Skovpen, S. Tavernier, W. Van Doninck, P. Van Mulders

Université Libre de Bruxelles, Bruxelles, Belgium
D. Beghin, B. Bilin, H. Brun, B. Clerbaux, G. De Lentdecker, H. Delannoy, B. Dorney, L. Favart, A. Grebenyuk, A.K. Kalsi, A. Popov, N. Postiau, E. Starling, L. Thomas, C. Vander Velde, P. Vanlaer, D. Vannerom

Ghent University, Ghent, Belgium
T. Cornelis, D. Dobur, I. Khvastunov[2], M. Niedziela, C. Roskas, D. Trocino, M. Tytgat, W. Verbeke, B. Vermassen, M. Vit, N. Zaganidis

Université Catholique de Louvain, Louvain-la-Neuve, Belgium
O. Bondu, G. Bruno, C. Caputo, P. David, C. Delaere, M. Delcourt, A. Giammanco, V. Lemaitre, A. Magitteri, J. Prisciandaro, A. Saggio, M. Vidal Marono, P. Vischia, J. Zobec

Centro Brasileiro de Pesquisas Fisicas, Rio de Janeiro, Brazil
F.L. Alves, G.A. Alves, G. Correia Silva, C. Hensel, A. Moraes, P. Rebello Teles

Universidade do Estado do Rio de Janeiro, Rio de Janeiro, Brazil
E. Belchior Batista Das Chagas, W. Carvalho, J. Chinellato[3], E. Coelho, E.M. Da Costa, G.G. Da Silveira[4], D. De Jesus Damiao, C. De Oliveira Martins, S. Fonseca De Souza, L.M. Huertas Guativa, H. Malbouisson, J. Martins[5], D. Matos Figueiredo, M. Medina Jaime[6], M. Melo De Almeida, C. Mora Herrera, L. Mundim, H. Nogima, W.L. Prado Da Silva, L.J. Sanchez Rosas, A. Santoro, A. Sznajder, M. Thiel, E.J. Tonelli Manganote[3], F. Torres Da Silva De Araujo, A. Vilela Pereira

Universidade Estadual Paulista [a], Universidade Federal do ABC [b], São Paulo, Brazil
C.A. Bernardes[a], L. Calligaris[a], T.R. Fernandez Perez Tomei[a], E.M. Gregores[b], D.S. Lemos, P.G. Mercadante[b], S.F. Novaes[a], SandraS. Padula[a]

Institute for Nuclear Research and Nuclear Energy, Bulgarian Academy of Sciences, Sofia, Bulgaria
A. Aleksandrov, G. Antchev, R. Hadjiiska, P. Iaydjiev, M. Misheva, M. Rodozov, M. Shopova, G. Sultanov

University of Sofia, Sofia, Bulgaria
M. Bonchev, A. Dimitrov, T. Ivanov, L. Litov, B. Pavlov, P. Petkov

Beihang University, Beijing, China
W. Fang[7], X. Gao[7], L. Yuan

Department of Physics, Tsinghua University, Beijing, China
Z. Hu, Y. Wang

Institute of High Energy Physics, Beijing, China
M. Ahmad, G.M. Chen, H.S. Chen, M. Chen, C.H. Jiang, D. Leggat, H. Liao, Z. Liu, S.M. Shaheen[8], A. Spiezia, J. Tao, E. Yazgan, H. Zhang, S. Zhang[8], J. Zhao

State Key Laboratory of Nuclear Physics and Technology, Peking University, Beijing, China
A. Agapitos, Y. Ban, G. Chen, A. Levin, J. Li, L. Li, Q. Li, Y. Mao, S.J. Qian, D. Wang, Q. Wang

Zhejiang University, Hangzhou, China
M. Xiao

Universidad de Los Andes, Bogota, Colombia
C. Avila, A. Cabrera, C. Florez, C.F. González Hernández, M.A. Segura Delgado

Universidad de Antioquia, Medellin, Colombia
J. Mejia Guisao, J.D. Ruiz Alvarez, C.A. Salazar González, N. Vanegas Arbelaez

University of Split, Faculty of Electrical Engineering, Mechanical Engineering and Naval Architecture, Split, Croatia
D. Giljanović, N. Godinovic, D. Lelas, I. Puljak, T. Sculac

University of Split, Faculty of Science, Split, Croatia
Z. Antunovic, M. Kovac

Institute Rudjer Boskovic, Zagreb, Croatia
V. Brigljevic, S. Ceci, D. Ferencek, K. Kadija, B. Mesic, M. Roguljic, A. Starodumov[9], T. Susa

University of Cyprus, Nicosia, Cyprus
M.W. Ather, A. Attikis, E. Erodotou, A. Ioannou, M. Kolosova, S. Konstantinou, G. Mavromanolakis, J. Mousa, C. Nicolaou, F. Ptochos, P.A. Razis, H. Rykaczewski, D. Tsiakkouri

Charles University, Prague, Czech Republic
M. Finger[10], M. Finger Jr.[10], A. Kveton, J. Tomsa

Escuela Politecnica Nacional, Quito, Ecuador
E. Ayala

Universidad San Francisco de Quito, Quito, Ecuador
E. Carrera Jarrin

Academy of Scientific Research and Technology of the Arab Republic of Egypt, Egyptian Network of High Energy Physics, Cairo, Egypt
Y. Assran[11,12], S. Elgammal[12]

National Institute of Chemical Physics and Biophysics, Tallinn, Estonia
S. Bhowmik, A. Carvalho Antunes De Oliveira, R.K. Dewanjee, K. Ehataht, M. Kadastik, M. Raidal, C. Veelken

Department of Physics, University of Helsinki, Helsinki, Finland
P. Eerola, L. Forthomme, H. Kirschenmann, K. Osterberg, M. Voutilainen

Helsinki Institute of Physics, Helsinki, Finland
F. Garcia, J. Havukainen, J.K. Heikkilä, T. Järvinen, V. Karimäki, M.S. Kim, R. Kinnunen, T. Lampén, K. Lassila-Perini, S. Laurila, S. Lehti, T. Lindén, P. Luukka, T. Mäenpää, H. Siikonen, E. Tuominen, J. Tuominiemi

Lappeenranta University of Technology, Lappeenranta, Finland
T. Tuuva

IRFU, CEA, Université Paris-Saclay, Gif-sur-Yvette, France
M. Besancon, F. Couderc, M. Dejardin, D. Denegri, B. Fabbro, J.L. Faure, F. Ferri, S. Ganjour, A. Givernaud, P. Gras, G. Hamel de Monchenault, P. Jarry, C. Leloup, E. Locci, J. Malcles, J. Rander, A. Rosowsky, M.Ö. Sahin, A. Savoy-Navarro[13], M. Titov

Laboratoire Leprince-Ringuet, CNRS/IN2P3, Ecole Polytechnique, Institut Polytechnique de Paris
S. Ahuja, C. Amendola, F. Beaudette, P. Busson, C. Charlot, B. Diab, G. Falmagne, R. Granier de Cassagnac, I. Kucher, A. Lobanov, C. Martin Perez, M. Nguyen, C. Ochando, P. Paganini, J. Rembser, R. Salerno, J.B. Sauvan, Y. Sirois, A. Zabi, A. Zghiche

Université de Strasbourg, CNRS, IPHC UMR 7178, Strasbourg, France
J.-L. Agram[14], J. Andrea, D. Bloch, G. Bourgatte, J.-M. Brom, E.C. Chabert, C. Collard, E. Conte[14], J.-C. Fontaine[14], D. Gelé, U. Goerlach, M. Jansová, A.-C. Le Bihan, N. Tonon, P. Van Hove

Centre de Calcul de l'Institut National de Physique Nucleaire et de Physique des Particules, CNRS/IN2P3, Villeurbanne, France
S. Gadrat

Université de Lyon, Université Claude Bernard Lyon 1, CNRS-IN2P3, Institut de Physique Nucléaire de Lyon, Villeurbanne, France
S. Beauceron, C. Bernet, G. Boudoul, C. Camen, A. Carle, N. Chanon, R. Chierici, D. Contardo, P. Depasse, H. El Mamouni, J. Fay, S. Gascon, M. Gouzevitch, B. Ille, Sa. Jain, F. Lagarde, I.B. Laktineh, H. Lattaud, A. Lesauvage, M. Lethuillier, L. Mirabito, S. Perries, V. Sordini, L. Torterotot, G. Touquet, M. Vander Donckt, S. Viret

Georgian Technical University, Tbilisi, Georgia
G. Adamov

Tbilisi State University, Tbilisi, Georgia
Z. Tsamalaidze[10]

RWTH Aachen University, I. Physikalisches Institut, Aachen, Germany
C. Autermann, L. Feld, M.K. Kiesel, K. Klein, M. Lipinski, D. Meuser, A. Pauls, M. Preuten, M.P. Rauch, C. Schomakers, J. Schulz, M. Teroerde, B. Wittmer

RWTH Aachen University, III. Physikalisches Institut A, Aachen, Germany
A. Albert, M. Erdmann, B. Fischer, S. Ghosh, T. Hebbeker, K. Hoepfner, H. Keller, L. Mastrolorenzo, M. Merschmeyer, A. Meyer, P. Millet, G. Mocellin, S. Mondal, S. Mukherjee, D. Noll, A. Novak, T. Pook, A. Pozdnyakov, T. Quast, M. Radziej, Y. Rath, H. Reithler, J. Roemer, A. Schmidt, S.C. Schuler, A. Sharma, S. Wiedenbeck, S. Zaleski

RWTH Aachen University, III. Physikalisches Institut B, Aachen, Germany
G. Flügge, W. Haj Ahmad[15], O. Hlushchenko, T. Kress, T. Müller, A. Nehrkorn, A. Nowack, C. Pistone, O. Pooth, D. Roy, H. Sert, A. Stahl[16]

Deutsches Elektronen-Synchrotron, Hamburg, Germany
M. Aldaya Martin, P. Asmuss, I. Babounikau, H. Bakhshiansohi, K. Beernaert, O. Behnke, A. Bermúdez Martínez, D. Bertsche, A.A. Bin Anuar, K. Borras[17], V. Botta, A. Campbell, A. Cardini, P. Connor, S. Consuegra Rodríguez, C. Contreras-Campana, V. Danilov, A. De Wit, M.M. Defranchis, C. Diez Pardos, D. Domínguez Damiani, G. Eckerlin, D. Eckstein, T. Eichhorn, A. Elwood, E. Eren, E. Gallo[18], A. Geiser, A. Grohsjean, M. Guthoff, M. Haranko, A. Harb, A. Jafari, N.Z. Jomhari, H. Jung, A. Kasem[17], M. Kasemann, H. Kaveh, J. Keaveney, C. Kleinwort, J. Knolle, D. Krücker, W. Lange, T. Lenz, J. Leonard, J. Lidrych, K. Lipka, W. Lohmann[19], R. Mankel, I.-A. Melzer-Pellmann, A.B. Meyer, M. Meyer, M. Missiroli, G. Mittag, J. Mnich, A. Mussgiller, V. Myronenko, D. Pérez Adán, S.K. Pflitsch, D. Pitzl, A. Raspereza, A. Saibel, M. Savitskyi, V. Scheurer, P. Schütze, C. Schwanenberger, R. Shevchenko, A. Singh, H. Tholen, O. Turkot, A. Vagnerini, M. Van De Klundert, R. Walsh, Y. Wen, K. Wichmann, C. Wissing, O. Zenaiev, R. Zlebcik

University of Hamburg, Hamburg, Germany
R. Aggleton, S. Bein, L. Benato, A. Benecke, V. Blobel, T. Dreyer, A. Ebrahimi, F. Feindt, A. Fröhlich, C. Garbers, E. Garutti, D. Gonzalez, P. Gunnellini, J. Haller, A. Hinzmann, A. Karavdina, G. Kasieczka, R. Kogler, N. Kovalchuk, S. Kurz, V. Kutzner, J. Lange, T. Lange, A. Malara, J. Multhaup, C.E.N. Niemeyer, A. Perieanu, A. Reimers, O. Rieger, C. Scharf, P. Schleper, S. Schumann, J. Schwandt, J. Sonneveld, H. Stadie, G. Steinbrück, F.M. Stober, M. Stöver, B. Vormwald, I. Zoi

Karlsruher Institut fuer Technologie, Karlsruhe, Germany
M. Akbiyik, C. Barth, M. Baselga, S. Baur, T. Berger, E. Butz, R. Caspart, T. Chwalek, W. De Boer, A. Dierlamm, K. El Morabit, N. Faltermann, M. Giffels, P. Goldenzweig, A. Gottmann, M.A. Harrendorf, F. Hartmann[16], U. Husemann, S. Kudella, S. Mitra, M.U. Mozer, D. Müller, Th. Müller, M. Musich, A. Nürnberg, G. Quast, K. Rabbertz, M. Schröder, I. Shvetsov, H.J. Simonis, R. Ulrich, M. Wassmer, M. Weber, C. Wöhrmann, R. Wolf

Institute of Nuclear and Particle Physics (INPP), NCSR Demokritos, Aghia Paraskevi, Greece
G. Anagnostou, P. Asenov, G. Daskalakis, T. Geralis, A. Kyriakis, D. Loukas, G. Paspalaki

National and Kapodistrian University of Athens, Athens, Greece
M. Diamantopoulou, G. Karathanasis, P. Kontaxakis, A. Manousakis-katsikakis, A. Panagiotou, I. Papavergou, N. Saoulidou, A. Stakia, K. Theofilatos, K. Vellidis, E. Vourliotis

National Technical University of Athens, Athens, Greece
G. Bakas, K. Kousouris, I. Papakrivopoulos, G. Tsipolitis

University of Ioánnina, Ioánnina, Greece
I. Evangelou, C. Foudas, P. Gianneios, P. Katsoulis, P. Kokkas, S. Mallios, K. Manitara, N. Manthos, I. Papadopoulos, J. Strologas, F.A. Triantis, D. Tsitsonis

MTA-ELTE Lendület CMS Particle and Nuclear Physics Group, Eötvös Loránd University, Budapest, Hungary
M. Bartók[20], R. Chudasama, M. Csanad, P. Major, K. Mandal, A. Mehta, M.I. Nagy, G. Pasztor, O. Surányi, G.I. Veres

Wigner Research Centre for Physics, Budapest, Hungary
G. Bencze, C. Hajdu, D. Horvath[21], F. Sikler, T.Á. Vámi, V. Veszpremi, G. Vesztergombi†

Institute of Nuclear Research ATOMKI, Debrecen, Hungary
N. Beni, S. Czellar, J. Karancsi[20], A. Makovec, J. Molnar, Z. Szillasi

Institute of Physics, University of Debrecen, Debrecen, Hungary
P. Raics, D. Teyssier, Z.L. Trocsanyi, B. Ujvari

Eszterhazy Karoly University, Karoly Robert Campus, Gyongyos, Hungary
T. Csorgo, W.J. Metzger, F. Nemes, T. Novak

Indian Institute of Science (IISc), Bangalore, India
S. Choudhury, J.R. Komaragiri, P.C. Tiwari

National Institute of Science Education and Research, HBNI, Bhubaneswar, India
S. Bahinipati[23], C. Kar, G. Kole, P. Mal, V.K. Muraleedharan Nair Bindhu, A. Nayak[24], D.K. Sahoo[23], S.K. Swain

Panjab University, Chandigarh, India
S. Bansal, S.B. Beri, V. Bhatnagar, S. Chauhan, R. Chawla, N. Dhingra, R. Gupta, A. Kaur, M. Kaur, S. Kaur, P. Kumari, M. Lohan, M. Meena, K. Sandeep, S. Sharma, J.B. Singh, A.K. Virdi, G. Walia

University of Delhi, Delhi, India
A. Bhardwaj, B.C. Choudhary, R.B. Garg, M. Gola, S. Keshri, Ashok Kumar, S. Malhotra, M. Naimuddin, P. Priyanka, K. Ranjan, Aashaq Shah, R. Sharma

Saha Institute of Nuclear Physics, HBNI, Kolkata, India
R. Bhardwaj[25], M. Bharti[25], R. Bhattacharya, S. Bhattacharya, U. Bhawandeep[25], D. Bhowmik, S. Dutta, S. Ghosh, M. Maity[26], K. Mondal, S. Nandan, A. Purohit, P.K. Rout, G. Saha, S. Sarkar, T. Sarkar[26], M. Sharan, B. Singh[25], S. Thakur[25]

Indian Institute of Technology Madras, Madras, India
P.K. Behera, P. Kalbhor, A. Muhammad, P.R. Pujahari, A. Sharma, A.K. Sikdar

Bhabha Atomic Research Centre, Mumbai, India
D. Dutta, V. Jha, V. Kumar, D.K. Mishra, P.K. Netrakanti, L.M. Pant, P. Shukla

Tata Institute of Fundamental Research-A, Mumbai, India
T. Aziz, M.A. Bhat, S. Dugad, G.B. Mohanty, P. Shingade, N. Sur, RavindraKumar Verma

Tata Institute of Fundamental Research-B, Mumbai, India
S. Banerjee, S. Bhattacharya, S. Chatterjee, P. Das, M. Guchait, S. Karmakar, M.M. Kolwalkar, S. Kumar, G. Majumder, K. Mazumdar, P. Patel, P. Pathare, M.R. Patil, N. Sahoo, S. Sawant

Indian Institute of Science Education and Research (IISER), Pune, India
S. Chauhan, S. Dube, V. Hegde, B. Kansal, A. Kapoor, K. Kothekar, S. Pandey, A. Rane, A. Rastogi, S. Sharma

Institute for Research in Fundamental Sciences (IPM), Tehran, Iran
S. Chenarani[27], E. Eskandari Tadavani, S.M. Etesami[27], M. Khakzad, M. Mohammadi Najafabadi, M. Naseri, F. Rezaei Hosseinabadi

University College Dublin, Dublin, Ireland
M. Felcini, M. Grunewald

INFN Sezione di Bari [a], Università di Bari [b], Politecnico di Bari [c], Bari, Italy
M. Abbrescia[a,b], R. Aly[a,b,28], C. Calabria[a,b], A. Colaleo[a], D. Creanza[a,c], L. Cristella[a,b], N. De Filippis[a,c], M. De Palma[a,b], A. Di Florio[a,b], L. Fiore[a], A. Gelmi[a,b], G. Iaselli[a,c], M. Ince[a,b], S. Lezki[a,b], G. Maggi[a,c], M. Maggi[a], G. Miniello[a,b], S. My[a,b], S. Nuzzo[a,b],

A. Pompili[a,b], G. Pugliese[a,c], R. Radogna[a], A. Ranieri[a], G. Selvaggi[a,b], L. Silvestris[a], R. Venditti[a], P. Verwilligen[a]

INFN Sezione di Bologna [a], Università di Bologna [b], Bologna, Italy
G. Abbiendi[a], C. Battilana[a,b], D. Bonacorsi[a,b], L. Borgonovi[a,b], S. Braibant-Giacomelli[a,b], R. Campanini[a,b], P. Capiluppi[a,b], A. Castro[a,b], F.R. Cavallo[a], C. Ciocca[a], G. Codispoti[a,b], M. Cuffiani[a,b], G.M. Dallavalle[a], F. Fabbri[a], A. Fanfani[a,b], E. Fontanesi[a,b], P. Giacomelli[a], C. Grandi[a], L. Guiducci[a,b], F. Iemmi[a,b], S. Lo Meo[a,29], S. Marcellini[a], G. Masetti[a], F.L. Navarria[a,b], A. Perrotta[a], F. Primavera[a,b], A.M. Rossi[a,b], T. Rovelli[a,b], G.P. Siroli[a,b], N. Tosi[a]

INFN Sezione di Catania [a], Università di Catania [b], Catania, Italy
S. Albergo[a,b,30], S. Costa[a,b], A. Di Mattia[a], R. Potenza[a,b], A. Tricomi[a,b,30], C. Tuve[a,b]

INFN Sezione di Firenze [a], Università di Firenze [b], Firenze, Italy
G. Barbagli[a], A. Cassese, R. Ceccarelli, K. Chatterjee[a,b], V. Ciulli[a,b], C. Civinini[a], R. D'Alessandro[a,b], E. Focardi[a,b], G. Latino[a,b], P. Lenzi[a,b], M. Meschini[a], S. Paoletti[a], G. Sguazzoni[a], L. Viliani[a]

INFN Laboratori Nazionali di Frascati, Frascati, Italy
L. Benussi, S. Bianco, D. Piccolo

INFN Sezione di Genova [a], Università di Genova [b], Genova, Italy
M. Bozzo[a,b], F. Ferro[a], R. Mulargia[a,b], E. Robutti[a], S. Tosi[a,b]

INFN Sezione di Milano-Bicocca [a], Università di Milano-Bicocca [b], Milano, Italy
A. Benaglia[a], A. Beschi[a,b], F. Brivio[a,b], V. Ciriolo[a,b,16], S. Di Guida[a,b,16], M.E. Dinardo[a,b], P. Dini[a], S. Gennai[a], A. Ghezzi[a,b], P. Govoni[a,b], L. Guzzi[a,b], M. Malberti[a], S. Malvezzi[a], D. Menasce[a], F. Monti[a,b], L. Moroni[a], M. Paganoni[a,b], D. Pedrini[a], S. Ragazzi[a,b], T. Tabarelli de Fatis[a,b], D. Zuolo[a,b]

INFN Sezione di Napoli [a], Università di Napoli 'Federico II' [b], Napoli, Italy, Università della Basilicata [c], Potenza, Italy, Università G. Marconi [d], Roma, Italy
S. Buontempo[a], N. Cavallo[a,c], A. De Iorio[a,b], A. Di Crescenzo[a,b], F. Fabozzi[a,c], F. Fienga[a], G. Galati[a], A.O.M. Iorio[a,b], L. Lista[a,b], S. Meola[a,d,16], P. Paolucci[a,16], B. Rossi[a], C. Sciacca[a,b], E. Voevodina[a,b]

INFN Sezione di Padova [a], Università di Padova [b], Padova, Italy, Università di Trento [c], Trento, Italy
P. Azzi[a], N. Bacchetta[a], D. Bisello[a,b], A. Boletti[a,b], A. Bragagnolo[a,b], R. Carlin[a,b], P. Checchia[a], P. De Castro Manzano[a], T. Dorigo[a], U. Dosselli[a], F. Gasparini[a,b], U. Gasparini[a,b], A. Gozzelino[a], S.Y. Hoh[a,b], P. Lujan[a], M. Margoni[a,b], A.T. Meneguzzo[a,b], J. Pazzini[a,b], M. Presilla[b], P. Ronchese[a,b], R. Rossin[a,b], F. Simonetto[a,b], A. Tiko[a], M. Tosi[a,b], M. Zanetti[a,b], P. Zotto[a,b], G. Zumerle[a,b]

INFN Sezione di Pavia [a], Università di Pavia [b], Pavia, Italy
A. Braghieri[a], D. Fiorina[a,b], P. Montagna[a,b], S.P. Ratti[a,b], V. Re[a], M. Ressegotti[a,b], C. Riccardi[a,b], P. Salvini[a], I. Vai[a], P. Vitulo[a,b]

INFN Sezione di Perugia [a], Università di Perugia [b], Perugia, Italy
M. Biasini[a,b], G.M. Bilei[a], D. Ciangottini[a,b], L. Fanò[a,b], P. Lariccia[a,b], R. Leonardi[a,b], G. Mantovani[a,b], V. Mariani[a,b], M. Menichelli[a], A. Rossi[a,b], A. Santocchia[a,b], D. Spiga[a]

INFN Sezione di Pisa [a], Università di Pisa [b], Scuola Normale Superiore di Pisa [c], Pisa, Italy
K. Androsov[a], P. Azzurri[a], G. Bagliesi[a], V. Bertacchi[a,c], L. Bianchini[a], T. Boccali[a], R. Castaldi[a], M.A. Ciocci[a,b], R. Dell'Orso[a], G. Fedi[a], L. Giannini[a,c], A. Giassi[a], M.T. Grippo[a],

F. Ligabue[a,c], E. Manca[a,c], G. Mandorli[a,c], A. Messineo[a,b], F. Palla[a], A. Rizzi[a,b], G. Rolandi[31], S. Roy Chowdhury, A. Scribano[a], P. Spagnolo[a], R. Tenchini[a], G. Tonelli[a,b], N. Turini, A. Venturi[a], P.G. Verdini[a]

INFN Sezione di Roma [a], Sapienza Università di Roma [b], Rome, Italy
F. Cavallari[a], M. Cipriani[a,b], D. Del Re[a,b], E. Di Marco[a,b], M. Diemoz[a], E. Longo[a,b], B. Marzocchi[a,b], P. Meridiani[a], G. Organtini[a,b], F. Pandolfi[a], R. Paramatti[a,b], C. Quaranta[a,b], S. Rahatlou[a,b], C. Rovelli[a], F. Santanastasio[a,b], L. Soffi[a,b]

INFN Sezione di Torino [a], Università di Torino [b], Torino, Italy, Università del Piemonte Orientale [c], Novara, Italy
N. Amapane[a,b], R. Arcidiacono[a,c], S. Argiro[a,b], M. Arneodo[a,c], N. Bartosik[a], R. Bellan[a,b], A. Bellora, C. Biino[a], A. Cappati[a,b], N. Cartiglia[a], S. Cometti[a], M. Costa[a,b], R. Covarelli[a,b], N. Demaria[a], B. Kiani[a,b], C. Mariotti[a], S. Maselli[a], E. Migliore[a,b], V. Monaco[a,b], E. Monteil[a,b], M. Monteno[a], M.M. Obertino[a,b], G. Ortona[a,b], L. Pacher[a,b], N. Pastrone[a], M. Pelliccioni[a], G.L. Pinna Angioni[a,b], A. Romero[a,b], M. Ruspa[a,c], R. Salvatico[a,b], V. Sola[a], A. Solano[a,b], D. Soldi[a,b], A. Staiano[a]

INFN Sezione di Trieste [a], Università di Trieste [b], Trieste, Italy
S. Belforte[a], V. Candelise[a,b], M. Casarsa[a], F. Cossutti[a], A. Da Rold[a,b], G. Della Ricca[a,b], F. Vazzoler[a,b], A. Zanetti[a]

Kyungpook National University, Daegu, Korea
B. Kim, D.H. Kim, G.N. Kim, J. Lee, S.W. Lee, C.S. Moon, Y.D. Oh, S.I. Pak, S. Sekmen, D.C. Son, Y.C. Yang

Chonnam National University, Institute for Universe and Elementary Particles, Kwangju, Korea
H. Kim, D.H. Moon, G. Oh

Hanyang University, Seoul, Korea
B. Francois, T.J. Kim, J. Park

Korea University, Seoul, Korea
S. Cho, S. Choi, Y. Go, D. Gyun, S. Ha, B. Hong, K. Lee, K.S. Lee, J. Lim, J. Park, S.K. Park, Y. Roh, J. Yoo

Kyung Hee University, Department of Physics
J. Goh

Sejong University, Seoul, Korea
H.S. Kim

Seoul National University, Seoul, Korea
J. Almond, J.H. Bhyun, J. Choi, S. Jeon, J. Kim, J.S. Kim, H. Lee, K. Lee, S. Lee, K. Nam, M. Oh, S.B. Oh, B.C. Radburn-Smith, U.K. Yang, H.D. Yoo, I. Yoon, G.B. Yu

University of Seoul, Seoul, Korea
D. Jeon, H. Kim, J.H. Kim, J.S.H. Lee, I.C. Park, I.J Watson

Sungkyunkwan University, Suwon, Korea
Y. Choi, C. Hwang, Y. Jeong, J. Lee, Y. Lee, I. Yu

Riga Technical University, Riga, Latvia
V. Veckalns[32]

Vilnius University, Vilnius, Lithuania
V. Dudenas, A. Juodagalvis, G. Tamulaitis, J. Vaitkus

National Centre for Particle Physics, Universiti Malaya, Kuala Lumpur, Malaysia
Z.A. Ibrahim, F. Mohamad Idris[33], W.A.T. Wan Abdullah, M.N. Yusli, Z. Zolkapli

Universidad de Sonora (UNISON), Hermosillo, Mexico
J.F. Benitez, A. Castaneda Hernandez, J.A. Murillo Quijada, L. Valencia Palomo

Centro de Investigacion y de Estudios Avanzados del IPN, Mexico City, Mexico
H. Castilla-Valdez, E. De La Cruz-Burelo, I. Heredia-De La Cruz[34], R. Lopez-Fernandez, A. Sanchez-Hernandez

Universidad Iberoamericana, Mexico City, Mexico
S. Carrillo Moreno, C. Oropeza Barrera, M. Ramirez-Garcia, F. Vazquez Valencia

Benemerita Universidad Autonoma de Puebla, Puebla, Mexico
J. Eysermans, I. Pedraza, H.A. Salazar Ibarguen, C. Uribe Estrada

Universidad Autónoma de San Luis Potosí, San Luis Potosí, Mexico
A. Morelos Pineda

University of Montenegro, Podgorica, Montenegro
J. Mijuskovic, N. Raicevic

University of Auckland, Auckland, New Zealand
D. Krofcheck

University of Canterbury, Christchurch, New Zealand
S. Bheesette, P.H. Butler

National Centre for Physics, Quaid-I-Azam University, Islamabad, Pakistan
A. Ahmad, M. Ahmad, Q. Hassan, H.R. Hoorani, W.A. Khan, M.A. Shah, M. Shoaib, M. Waqas

AGH University of Science and Technology Faculty of Computer Science, Electronics and Telecommunications, Krakow, Poland
V. Avati, L. Grzanka, M. Malawski

National Centre for Nuclear Research, Swierk, Poland
H. Bialkowska, M. Bluj, B. Boimska, M. Górski, M. Kazana, M. Szleper, P. Zalewski

Institute of Experimental Physics, Faculty of Physics, University of Warsaw, Warsaw, Poland
K. Bunkowski, A. Byszuk[35], K. Doroba, A. Kalinowski, M. Konecki, J. Krolikowski, M. Misiura, M. Olszewski, M. Walczak

Laboratório de Instrumentação e Física Experimental de Partículas, Lisboa, Portugal
M. Araujo, P. Bargassa, D. Bastos, A. Di Francesco, P. Faccioli, B. Galinhas, M. Gallinaro, J. Hollar, N. Leonardo, J. Seixas, K. Shchelina, G. Strong, O. Toldaiev, J. Varela

Joint Institute for Nuclear Research, Dubna, Russia
S. Afanasiev, P. Bunin, M. Gavrilenko, I. Golutvin, I. Gorbunov, A. Kamenev, V. Karjavine, A. Lanev, A. Malakhov, V. Matveev[36,37], P. Moisenz, V. Palichik, V. Perelygin, M. Savina, S. Shmatov, S. Shulha, N. Skatchkov, V. Smirnov, N. Voytishin, A. Zarubin

Petersburg Nuclear Physics Institute, Gatchina (St. Petersburg), Russia
L. Chtchipounov, V. Golovtcov, Y. Ivanov, V. Kim[38], E. Kuznetsova[39], P. Levchenko, V. Murzin, V. Oreshkin, I. Smirnov, D. Sosnov, V. Sulimov, L. Uvarov, A. Vorobyev

Institute for Nuclear Research, Moscow, Russia
Yu. Andreev, A. Dermenev, S. Gninenko, N. Golubev, A. Karneyeu, M. Kirsanov, N. Krasnikov, A. Pashenkov, D. Tlisov, A. Toropin

Institute for Theoretical and Experimental Physics named by A.I. Alikhanov of NRC 'Kurchatov Institute', Moscow, Russia
V. Epshteyn, V. Gavrilov, N. Lychkovskaya, A. Nikitenko[40], V. Popov, I. Pozdnyakov, G. Safronov, A. Spiridonov, A. Stepennov, M. Toms, E. Vlasov, A. Zhokin

Moscow Institute of Physics and Technology, Moscow, Russia
T. Aushev

National Research Nuclear University 'Moscow Engineering Physics Institute' (MEPhI), Moscow, Russia
M. Chadeeva[41], R. Chistov[41], M. Danilov[41], P. Parygin, D. Philippov, S. Polikarpov[41], E. Popova, V. Rusinov, E. Tarkovskii

P.N. Lebedev Physical Institute, Moscow, Russia
V. Andreev, M. Azarkin, I. Dremin, M. Kirakosyan, A. Terkulov

Skobeltsyn Institute of Nuclear Physics, Lomonosov Moscow State University, Moscow, Russia
A. Belyaev, E. Boos, A. Demiyanov, L. Dudko, A. Ershov, A. Gribushin, A. Kaminskiy[42], V. Klyukhin, O. Kodolova, I. Lokhtin, S. Obraztsov, S. Petrushanko, V. Savrin

Novosibirsk State University (NSU), Novosibirsk, Russia
A. Barnyakov[43], V. Blinov[43], T. Dimova[43], L. Kardapoltsev[43], Y. Skovpen[43]

Institute for High Energy Physics of National Research Centre 'Kurchatov Institute', Protvino, Russia
I. Azhgirey, I. Bayshev, S. Bitioukov, V. Kachanov, D. Konstantinov, P. Mandrik, V. Petrov, R. Ryutin, S. Slabospitskii, A. Sobol, S. Troshin, N. Tyurin, A. Uzunian, A. Volkov

National Research Tomsk Polytechnic University, Tomsk, Russia
A. Babaev, A. Iuzhakov, V. Okhotnikov

Tomsk State University, Tomsk, Russia
V. Borchsh, V. Ivanchenko, E. Tcherniaev

University of Belgrade: Faculty of Physics and VINCA Institute of Nuclear Sciences
P. Adzic[44], P. Cirkovic, D. Devetak, M. Dordevic, P. Milenovic, J. Milosevic, M. Stojanovic

Centro de Investigaciones Energéticas Medioambientales y Tecnológicas (CIEMAT), Madrid, Spain
M. Aguilar-Benitez, J. Alcaraz Maestre, A. Álvarez Fernández, I. Bachiller, M. Barrio Luna, J.A. Brochero Cifuentes, C.A. Carrillo Montoya, M. Cepeda, M. Cerrada, N. Colino, B. De La Cruz, A. Delgado Peris, C. Fernandez Bedoya, J.P. Fernández Ramos, J. Flix, M.C. Fouz, O. Gonzalez Lopez, S. Goy Lopez, J.M. Hernandez, M.I. Josa, D. Moran, Á. Navarro Tobar, A. Pérez-Calero Yzquierdo, J. Puerta Pelayo, I. Redondo, L. Romero, S. Sánchez Navas, M.S. Soares, A. Triossi, C. Willmott

Universidad Autónoma de Madrid, Madrid, Spain
C. Albajar, J.F. de Trocóniz, R. Reyes-Almanza

Universidad de Oviedo, Instituto Universitario de Ciencias y Tecnologías Espaciales de Asturias (ICTEA), Oviedo, Spain
B. Alvarez Gonzalez, J. Cuevas, C. Erice, J. Fernandez Menendez, S. Folgueras, I. Gonzalez Caballero, J.R. González Fernández, E. Palencia Cortezon, V. Rodríguez Bouza, S. Sanchez Cruz

Instituto de Física de Cantabria (IFCA), CSIC-Universidad de Cantabria, Santander, Spain
I.J. Cabrillo, A. Calderon, B. Chazin Quero, J. Duarte Campderros, M. Fernandez, P.J. Fernández Manteca, A. García Alonso, G. Gomez, C. Martinez Rivero, P. Martinez Ruiz del Arbol, F. Matorras, J. Piedra Gomez, C. Prieels, T. Rodrigo, A. Ruiz-Jimeno, L. Russo[45], L. Scodellaro, N. Trevisani, I. Vila, J.M. Vizan Garcia

University of Colombo, Colombo, Sri Lanka
K. Malagalage

University of Ruhuna, Department of Physics, Matara, Sri Lanka
W.G.D. Dharmaratna, N. Wickramage

CERN, European Organization for Nuclear Research, Geneva, Switzerland
D. Abbaneo, B. Akgun, E. Auffray, G. Auzinger, J. Baechler, P. Baillon, A.H. Ball, D. Barney, J. Bendavid, M. Bianco, A. Bocci, P. Bortignon, E. Bossini, C. Botta, E. Brondolin, T. Camporesi, A. Caratelli, G. Cerminara, E. Chapon, G. Cucciati, D. d'Enterria, A. Dabrowski, N. Daci, V. Daponte, A. David, O. Davignon, A. De Roeck, N. Deelen, M. Deile, M. Dobson, M. Dünser, N. Dupont, A. Elliott-Peisert, N. Emriskova, F. Fallavollita[46], D. Fasanella, S. Fiorendi, G. Franzoni, J. Fulcher, W. Funk, S. Giani, D. Gigi, A. Gilbert, K. Gill, F. Glege, M. Gruchala, M. Guilbaud, D. Gulhan, J. Hegeman, C. Heidegger, Y. Iiyama, V. Innocente, P. Janot, O. Karacheban[19], J. Kaspar, J. Kieseler, M. Krammer[1], N. Kratochwil, C. Lange, P. Lecoq, C. Lourenço, L. Malgeri, M. Mannelli, A. Massironi, F. Meijers, J.A. Merlin, S. Mersi, E. Meschi, F. Moortgat, M. Mulders, J. Ngadiuba, J. Niedziela, S. Nourbakhsh, S. Orfanelli, L. Orsini, F. Pantaleo[16], L. Pape, E. Perez, M. Peruzzi, A. Petrilli, G. Petrucciani, A. Pfeiffer, M. Pierini, F.M. Pitters, D. Rabady, A. Racz, M. Rieger, M. Rovere, H. Sakulin, C. Schäfer, C. Schwick, M. Selvaggi, A. Sharma, P. Silva, W. Snoeys, P. Sphicas[47], J. Steggemann, S. Summers, V.R. Tavolaro, D. Treille, A. Tsirou, G.P. Van Onsem, A. Vartak, M. Verzetti, W.D. Zeuner

Paul Scherrer Institut, Villigen, Switzerland
L. Caminada[48], K. Deiters, W. Erdmann, R. Horisberger, Q. Ingram, H.C. Kaestli, D. Kotlinski, U. Langenegger, T. Rohe, S.A. Wiederkehr

ETH Zurich - Institute for Particle Physics and Astrophysics (IPA), Zurich, Switzerland
M. Backhaus, P. Berger, N. Chernyavskaya, G. Dissertori, M. Dittmar, M. Donegà, C. Dorfer, T.A. Gómez Espinosa, C. Grab, D. Hits, T. Klijnsma, W. Lustermann, R.A. Manzoni, M. Marionneau, M.T. Meinhard, F. Micheli, P. Musella, F. Nessi-Tedaldi, F. Pauss, G. Perrin, L. Perrozzi, S. Pigazzini, M.G. Ratti, M. Reichmann, C. Reissel, T. Reitenspiess, D. Ruini, D.A. Sanz Becerra, M. Schönenberger, L. Shchutska, M.L. Vesterbacka Olsson, R. Wallny, D.H. Zhu

Universität Zürich, Zurich, Switzerland
T.K. Aarrestad, C. Amsler[49], D. Brzhechko, M.F. Canelli, A. De Cosa, R. Del Burgo, S. Donato, B. Kilminster, S. Leontsinis, V.M. Mikuni, I. Neutelings, G. Rauco, P. Robmann, D. Salerno, K. Schweiger, C. Seitz, Y. Takahashi, S. Wertz, A. Zucchetta

National Central University, Chung-Li, Taiwan
T.H. Doan, C.M. Kuo, W. Lin, A. Roy, S.S. Yu

National Taiwan University (NTU), Taipei, Taiwan
P. Chang, Y. Chao, K.F. Chen, P.H. Chen, W.-S. Hou, Y.y. Li, R.-S. Lu, E. Paganis, A. Psallidas, A. Steen

Chulalongkorn University, Faculty of Science, Department of Physics, Bangkok, Thailand
B. Asavapibhop, C. Asawatangtrakuldee, N. Srimanobhas, N. Suwonjandee

Çukurova University, Physics Department, Science and Art Faculty, Adana, Turkey
D. Agyel, S. Anagul, M.N. Bakirci[50], A. Bat, F. Bilican, F. Boran, A. Celik[51], S. Cerci[52], S. Damarseckin[53], Z.S. Demiroglu, F. Dolek, C. Dozen, I. Dumanoglu, G. Gokbulut, EmineGurpinar Guler[54], Y. Guler, I. Hos[55], C. Isik, E.E. Kangal[56], O. Kara, A. Kayis Topaksu, U. Kiminsu, M. Oglakci, G. Onengut, K. Ozdemir[57], S. Ozturk[50], A.E. Simsek, . Sözbilir, D. Sunar Cerci[52], B. Tali[52], U.G. Tok, H. Topakli[50], S. Turkcapar, E. Uslan, I.S. Zorbakir, C. Zorbilmez

Middle East Technical University, Physics Department, Ankara, Turkey
B. Isildak[58], G. Karapinar[59], M. Yalvac

Bogazici University, Istanbul, Turkey
I.O. Atakisi, E. Gülmez, M. Kaya[60], O. Kaya[61], Ö. Özçelik, S. Tekten, E.A. Yetkin[62]

Istanbul Technical University, Istanbul, Turkey
A. Cakir, K. Cankocak, Y. Komurcu, S. Sen[63]

Istanbul University, Istanbul, Turkey
B. Kaynak, S. Ozkorucuklu

Institute for Scintillation Materials of National Academy of Science of Ukraine, Kharkov, Ukraine
B. Grynyov

National Scientific Center, Kharkov Institute of Physics and Technology, Kharkov, Ukraine
L. Levchuk, V. Popov

University of Bristol, Bristol, United Kingdom
F. Ball, E. Bhal, S. Bologna, J.J. Brooke, D. Burns[64], E. Clement, D. Cussans, H. Flacher, J. Goldstein, G.P. Heath, H.F. Heath, L. Kreczko, S. Paramesvaran, B. Penning, T. Sakuma, S. Seif El Nasr-Storey, V.J. Smith, J. Taylor, A. Titterton

Rutherford Appleton Laboratory, Didcot, United Kingdom
K.W. Bell, A. Belyaev[65], C. Brew, R.M. Brown, D. Cieri, D.J.A. Cockerill, J.A. Coughlan, K. Harder, S. Harper, J. Linacre, K. Manolopoulos, D.M. Newbold, E. Olaiya, D. Petyt, T. Reis, T. Schuh, C.H. Shepherd-Themistocleous, A. Thea, I.R. Tomalin, T. Williams, W.J. Womersley

Imperial College, London, United Kingdom
R. Bainbridge, P. Bloch, J. Borg, S. Breeze, O. Buchmuller, A. Bundock, GurpreetSingh CHAHAL[66], D. Colling, P. Dauncey, G. Davies, M. Della Negra, R. Di Maria, P. Everaerts, G. Hall, G. Iles, T. James, M. Komm, C. Laner, L. Lyons, A.-M. Magnan, S. Malik, A. Martelli, V. Milosevic, J. Nash[67], V. Palladino, M. Pesaresi, D.M. Raymond, A. Richards, A. Rose, E. Scott, C. Seez, A. Shtipliyski, M. Stoye, T. Strebler, A. Tapper, K. Uchida, T. Virdee[16], N. Wardle, D. Winterbottom, J. Wright, A.G. Zecchinelli, S.C. Zenz

Brunel University, Uxbridge, United Kingdom
J.E. Cole, P.R. Hobson, A. Khan, P. Kyberd, C.K. Mackay, A. Morton, I.D. Reid, L. Teodorescu, S. Zahid

Baylor University, Waco, USA
K. Call, B. Caraway, J. Dittmann, K. Hatakeyama, C. Madrid, B. McMaster, N. Pastika, C. Smith

Catholic University of America, Washington, DC, USA
R. Bartek, A. Dominguez, R. Uniyal, A.M. Vargas Hernandez

The University of Alabama, Tuscaloosa, USA
A. Buccilli, S.I. Cooper, C. Henderson, P. Rumerio, C. West

Boston University, Boston, USA
D. Arcaro, C. Cosby, Z. Demiragli, D. Gastler, E. Hazen, D. Pinna, C. Richardson, J. Rohlf, D. Sperka, I. Suarez, L. Sulak, S. Wu, D. Zou

Brown University, Providence, USA
G. Benelli, B. Burkle, X. Coubez[17], D. Cutts, Y.t. Duh, M. Hadley, J. Hakala, U. Heintz, J.M. Hogan[68], K.H.M. Kwok, E. Laird, G. Landsberg, J. Lee, Z. Mao, M. Narain, S. Sagir[69], R. Syarif, E. Usai, D. Yu, W. Zhang

University of California, Davis, Davis, USA
R. Band, C. Brainerd, R. Breedon, M. Calderon De La Barca Sanchez, M. Chertok, J. Conway, R. Conway, P.T. Cox, R. Erbacher, C. Flores, G. Funk, F. Jensen, W. Ko, O. Kukral, R. Lander, M. Mulhearn, D. Pellett, J. Pilot, M. Shi, D. Taylor, K. Tos, M. Tripathi, Z. Wang, F. Zhang

University of California, Los Angeles, USA
M. Bachtis, C. Bravo, R. Cousins, A. Dasgupta, A. Florent, J. Hauser, M. Ignatenko, N. Mccoll, W.A. Nash, S. Regnard, D. Saltzberg, C. Schnaible, B. Stone, V. Valuev

University of California, Riverside, Riverside, USA
K. Burt, Y. Chen, R. Clare, J.W. Gary, S.M.A. Ghiasi Shirazi, G. Hanson, G. Karapostoli, E. Kennedy, O.R. Long, M. Olmedo Negrete, M.I. Paneva, W. Si, L. Wang, S. Wimpenny, B.R. Yates, Y. Zhang

University of California, San Diego, La Jolla, USA
J.G. Branson, P. Chang, S. Cittolin, M. Derdzinski, R. Gerosa, D. Gilbert, B. Hashemi, D. Klein, V. Krutelyov, J. Letts, M. Masciovecchio, S. May, S. Padhi, M. Pieri, V. Sharma, M. Tadel, F. Würthwein, A. Yagil, G. Zevi Della Porta

University of California, Santa Barbara - Department of Physics, Santa Barbara, USA
N. Amin, R. Bhandari, C. Campagnari, M. Citron, V. Dutta, M. Franco Sevilla, L. Gouskos, J. Incandela, B. Marsh, H. Mei, A. Ovcharova, H. Qu, J. Richman, U. Sarica, D. Stuart, S. Wang

California Institute of Technology, Pasadena, USA
D. Anderson, A. Bornheim, O. Cerri, I. Dutta, J.M. Lawhorn, N. Lu, J. Mao, H.B. Newman, T.Q. Nguyen, J. Pata, M. Spiropulu, J.R. Vlimant, S. Xie, Z. Zhang, R.Y. Zhu

Carnegie Mellon University, Pittsburgh, USA
M.B. Andrews, T. Ferguson, T. Mudholkar, M. Paulini, M. Sun, I. Vorobiev, M. Weinberg

University of Colorado Boulder, Boulder, USA
J.P. Cumalat, W.T. Ford, A. Johnson, E. MacDonald, T. Mulholland, R. Patel, A. Perloff, K. Stenson, K.A. Ulmer, S.R. Wagner

Cornell University, Ithaca, USA
J. Alexander, J. Chaves, Y. Cheng, J. Chu, A. Datta, A. Frankenthal, K. Mcdermott, J.R. Patterson, D. Quach, A. Rinkevicius[70], A. Ryd, S.M. Tan, Z. Tao, J. Thom, P. Wittich, M. Zientek

Fairfield University, Fairfield, USA
D. Winn

Fermi National Accelerator Laboratory, Batavia, USA
S. Abdullin, M. Albrow, M. Alyari, G. Apollinari, A. Apresyan, A. Apyan, S. Banerjee, L.A.T. Bauerdick, A. Beretvas, J. Berryhill, P.C. Bhat, K. Burkett, J.N. Butler, A. Canepa, G.B. Cerati, H.W.K. Cheung, F. Chlebana, M. Cremonesi, J. Duarte, V.D. Elvira, J. Freeman, Z. Gecse, E. Gottschalk, L. Gray, D. Green, S. Grünendahl, O. Gutsche, AllisonReinsvold Hall, J. Hanlon, R.M. Harris, S. Hasegawa, R. Heller, J. Hirschauer, B. Jayatilaka, S. Jindariani, M. Johnson, U. Joshi, B. Klima, M.J. Kortelainen, B. Kreis, S. Lammel, J. Lewis, D. Lincoln, R. Lipton, M. Liu, T. Liu, J. Lykken, K. Maeshima, J.M. Marraffino, D. Mason, P. McBride, P. Merkel, S. Mrenna, S. Nahn, V. O'Dell, V. Papadimitriou, K. Pedro, C. Pena, G. Rakness, F. Ravera, L. Ristori, B. Schneider, E. Sexton-Kennedy, N. Smith, A. Soha, W.J. Spalding, L. Spiegel, S. Stoynev, J. Strait, N. Strobbe, L. Taylor, S. Tkaczyk, N.V. Tran, L. Uplegger, E.W. Vaandering, C. Vernieri, R. Vidal, M. Wang, H.A. Weber

University of Florida, Gainesville, USA
D. Acosta, P. Avery, D. Bourilkov, A. Brinkerhoff, L. Cadamuro, A. Carnes, V. Cherepanov, D. Curry, F. Errico, R.D. Field, S.V. Gleyzer, B.M. Joshi, M. Kim, J. Konigsberg, A. Korytov, K.H. Lo, P. Ma, K. Matchev, N. Menendez, G. Mitselmakher, D. Rosenzweig, K. Shi, J. Wang, S. Wang, X. Zuo

Florida International University, Miami, USA
Y.R. Joshi

Florida State University, Tallahassee, USA
T. Adams, A. Askew, S. Hagopian, V. Hagopian, K.F. Johnson, R. Khurana, T. Kolberg, G. Martinez, T. Perry, H. Prosper, C. Schiber, R. Yohay, J. Zhang

Florida Institute of Technology, Melbourne, USA
M.M. Baarmand, M. Hohlmann, D. Noonan, M. Rahmani, M. Saunders, F. Yumiceva

University of Illinois at Chicago (UIC), Chicago, USA
M.R. Adams, L. Apanasevich, D. Berry, R.R. Betts, R. Cavanaugh, X. Chen, S. Dittmer, O. Evdokimov, C.E. Gerber, D.A. Hangal, D.J. Hofman, K. Jung, C. Mills, T. Roy, M.B. Tonjes, N. Varelas, J. Viinikainen, H. Wang, X. Wang, Z. Wu

The University of Iowa, Iowa City, USA
M. Alhusseini, B. Bilki[54], W. Clarida, P. Debbins, K. Dilsiz[71], S. Durgut, L. Emediato, R.P. Gandrajula, M. Haytmyradov, V. Khristenko, O.K. Köseyan, T. Mcdowell, J.-P. Merlo, A. Mestvirishvili[72], M.J. Miller, A. Moeller, J. Nachtman, H. Ogul[73], Y. Onel, F. Ozok[74], A. Penzo, C. Rude, I. Schmidt, C. Snyder, D. Southwick, E. Tiras, J. Wetzel, K. Yi[75]

Johns Hopkins University, Baltimore, USA
B. Blumenfeld, A. Cocoros, N. Eminizer, D. Fehling, L. Feng, A.V. Gritsan, W.T. Hung, P. Maksimovic, J. Roskes, M. Swartz

The University of Kansas, Lawrence, USA
C. Baldenegro Barrera, P. Baringer, A. Bean, S. Boren, J. Bowen, A. Bylinkin, T. Isidori, S. Khalil, J. King, G. Krintiras, A. Kropivnitskaya, C. Lindsey, D. Majumder, W. Mcbrayer, N. Minafra, M. Murray, C. Rogan, C. Royon, S. Sanders, E. Schmitz, J.D. Tapia Takaki, Q. Wang, J. Williams, G. Wilson

Kansas State University, Manhattan, USA
S. Duric, A. Ivanov, K. Kaadze, D. Kim, Y. Maravin, D.R. Mendis, T. Mitchell, A. Modak, A. Mohammadi

Lawrence Livermore National Laboratory, Livermore, USA
F. Rebassoo, D. Wright

University of Maryland, College Park, USA
A. Baden, O. Baron, A. Belloni, T. Edberg, S.C. Eno, Y. Feng, T. Grassi, N.J. Hadley, J. Hipkins, S. Jabeen, G.Y. Jeng, R.G. Kellogg, J. Kunkle, A.C. Mignerey, J. Muessig, S. Nabili, F. Ricci-Tam, M. Seidel, Y.H. Shin, A. Skuja, C. Sylber, S.C. Tonwar, K. Wong

Massachusetts Institute of Technology, Cambridge, USA
D. Abercrombie, B. Allen, A. Baty, R. Bi, S. Brandt, W. Busza, I.A. Cali, M. D'Alfonso, G. Gomez Ceballos, M. Goncharov, P. Harris, D. Hsu, M. Hu, M. Klute, D. Kovalskyi, Y.-J. Lee, P.D. Luckey, B. Maier, A.C. Marini, C. Mcginn, C. Mironov, S. Narayanan, X. Niu, C. Paus, D. Rankin, C. Roland, G. Roland, Z. Shi, G.S.F. Stephans, K. Sumorok, K. Tatar, D. Velicanu, J. Wang, T.W. Wang, B. Wyslouch

University of Minnesota, Minneapolis, USA
A.C. Benvenuti[†], R.M. Chatterjee, A. Evans, S. Guts, P. Hansen, J. Hiltbrand, Sh. Jain, Y. Kubota, Z. Lesko, J. Mans, R. Rusack, M.A. Wadud

University of Mississippi, Oxford, USA
J.G. Acosta, S. Oliveros

University of Nebraska-Lincoln, Lincoln, USA
K. Bloom, D.R. Claes, C. Fangmeier, L. Finco, F. Golf, R. Gonzalez Suarez, R. Kamalieddin, I. Kravchenko, J.E. Siado, G.R. Snow[†], B. Stieger, W. Tabb

State University of New York at Buffalo, Buffalo, USA
G. Agarwal, C. Harrington, I. Iashvili, A. Kharchilava, C. McLean, D. Nguyen, A. Parker, J. Pekkanen, S. Rappoccio, B. Roozbahani

Northeastern University, Boston, USA
G. Alverson, E. Barberis, C. Freer, Y. Haddad, A. Hortiangtham, G. Madigan, D.M. Morse, T. Orimoto, L. Skinnari, A. Tishelman-Charny, T. Wamorkar, B. Wang, A. Wisecarver, D. Wood

Northwestern University, Evanston, USA
S. Bhattacharya, J. Bueghly, T. Gunter, K.A. Hahn, N. Odell, M.H. Schmitt, K. Sung, M. Trovato, M. Velasco

University of Notre Dame, Notre Dame, USA
R. Bucci, N. Dev, R. Goldouzian, A.H. Heering, M. Hildreth, K. Hurtado Anampa, C. Jessop, D.J. Karmgard, K. Lannon, W. Li, N. Loukas, N. Marinelli, I. Mcalister, F. Meng, C. Mueller, Y. Musienko[36], M. Planer, R. Ruchti, P. Siddireddy, G. Smith, S. Taroni, M. Wayne, A. Wightman, M. Wolf, A. Woodard

The Ohio State University, Columbus, USA
J. Alimena, B. Bylsma, L.S. Durkin, S. Flowers, B. Francis, C. Hill, W. Ji, A. Lefeld, T.Y. Ling, B.L. Winer

Princeton University, Princeton, USA
S. Cooperstein, G. Dezoort, P. Elmer, J. Hardenbrook, N. Haubrich, S. Higginbotham,

A. Kalogeropoulos, S. Kwan, D. Lange, M.T. Lucchini, J. Luo, D. Marlow, K. Mei, I. Ojalvo, J. Olsen, C. Palmer, P. Piroué, J. Salfeld-Nebgen, D. Stickland, C. Tully, Z. Wang

University of Puerto Rico, Mayaguez, USA
S. Malik, S. Norberg

Purdue University, West Lafayette, USA
A. Barker, V.E. Barnes, S. Das, L. Gutay, M. Jones, A.W. Jung, A. Khatiwada, B. Mahakud, D.H. Miller, G. Negro, N. Neumeister, C.C. Peng, S. Piperov, H. Qiu, J.F. Schulte, J. Sun, F. Wang, R. Xiao, W. Xie

Purdue University Northwest, Hammond, USA
T. Cheng, J. Dolen, N. Parashar

Rice University, Houston, USA
U. Behrens, K.M. Ecklund, S. Freed, F.J.M. Geurts, M. Kilpatrick, Arun Kumar, W. Li, B.P. Padley, R. Redjimi, J. Roberts, J. Rorie, W. Shi, A.G. Stahl Leiton, Z. Tu, A. Zhang

University of Rochester, Rochester, USA
A. Bodek, P. de Barbaro, R. Demina, J.L. Dulemba, C. Fallon, T. Ferbel, M. Galanti, A. Garcia-Bellido, O. Hindrichs, A. Khukhunaishvili, E. Ranken, C.L. Tan, P. Tan, R. Taus, M. Zielinski

The Rockefeller University, New York, USA
R. Ciesielski

Rutgers, The State University of New Jersey, Piscataway, USA
B. Chiarito, J.P. Chou, A. Gandrakota, Y. Gershtein, E. Halkiadakis, A. Hart, M. Heindl, E. Hughes, S. Kaplan, S. Kyriacou, I. Laflotte, A. Lath, R. Montalvo, K. Nash, M. Osherson, H. Saka, S. Salur, S. Schnetzer, S. Somalwar, R. Stone, S. Thomas

University of Tennessee, Knoxville, USA
H. Acharya, A.G. Delannoy, G. Riley, S. Spanier

Texas A&M University, College Station, USA
O. Bouhali[76], M. Dalchenko, M. De Mattia, A. Delgado, S. Dildick, R. Eusebi, J. Gilmore, T. Huang, T. Kamon[77], S. Luo, D. Marley, R. Mueller, D. Overton, L. Perniè, D. Rathjens, A. Safonov

Texas Tech University, Lubbock, USA
N. Akchurin, J. Damgov, F. De Guio, S. Kunori, K. Lamichhane, S.W. Lee, T. Mengke, S. Muthumuni, T. Peltola, S. Undleeb, I. Volobouev, Z. Wang, A. Whitbeck

Vanderbilt University, Nashville, USA
S. Greene, A. Gurrola, R. Janjam, W. Johns, C. Maguire, A. Melo, H. Ni, K. Padeken, F. Romeo, P. Sheldon, S. Tuo, J. Velkovska, M. Verweij

University of Virginia, Charlottesville, USA
M.W. Arenton, P. Barria, B. Cox, G. Cummings, R. Hirosky, M. Joyce, A. Ledovskoy, C. Neu, B. Tannenwald, Y. Wang, E. Wolfe, F. Xia

Wayne State University, Detroit, USA
R. Harr, P.E. Karchin, N. Poudyal, J. Sturdy, P. Thapa

University of Wisconsin - Madison, Madison, WI, USA
T. Bose, J. Buchanan, C. Caillol, D. Carlsmith, S. Dasu, I. De Bruyn, L. Dodd, F. Fiori, C. Galloni, B. Gomber[78], H. He, M. Herndon, A. Hervé, U. Hussain, P. Klabbers, A. Lanaro, A. Loeliger,

K. Long, R. Loveless, J. Madhusudanan Sreekala, T. Ruggles, A. Savin, V. Sharma, W.H. Smith, D. Teague, S. Trembath-reichert, N. Woods

†: Deceased
1: Also at Vienna University of Technology, Vienna, Austria
2: Also at IRFU, CEA, Université Paris-Saclay, Gif-sur-Yvette, France
3: Also at Universidade Estadual de Campinas, Campinas, Brazil
4: Also at Federal University of Rio Grande do Sul, Porto Alegre, Brazil
5: Also at UFMS, Nova Andradina, Brazil
6: Also at Universidade Federal de Pelotas, Pelotas, Brazil
7: Also at Université Libre de Bruxelles, Bruxelles, Belgium
8: Also at University of Chinese Academy of Sciences, Beijing, China
9: Also at Institute for Theoretical and Experimental Physics named by A.I. Alikhanov of NRC 'Kurchatov Institute', Moscow, Russia
10: Also at Joint Institute for Nuclear Research, Dubna, Russia
11: Also at Suez University, Suez, Egypt
12: Now at British University in Egypt, Cairo, Egypt
13: Also at Purdue University, West Lafayette, USA
14: Also at Université de Haute Alsace, Mulhouse, France
15: Also at Erzincan Binali Yildirim University, Erzincan, Turkey
16: Also at CERN, European Organization for Nuclear Research, Geneva, Switzerland
17: Also at RWTH Aachen University, III. Physikalisches Institut A, Aachen, Germany
18: Also at University of Hamburg, Hamburg, Germany
19: Also at Brandenburg University of Technology, Cottbus, Germany
20: Also at Institute of Physics, University of Debrecen, Debrecen, Hungary, Debrecen, Hungary
21: Also at Institute of Nuclear Research ATOMKI, Debrecen, Hungary
22: Also at MTA-ELTE Lendület CMS Particle and Nuclear Physics Group, Eötvös Loránd University, Budapest, Hungary, Budapest, Hungary
23: Also at IIT Bhubaneswar, Bhubaneswar, India, Bhubaneswar, India
24: Also at Institute of Physics, Bhubaneswar, India
25: Also at Shoolini University, Solan, India
26: Also at University of Visva-Bharati, Santiniketan, India
27: Also at Isfahan University of Technology, Isfahan, Iran
28: Now at INFN Sezione di Bari [a], Università di Bari [b], Politecnico di Bari [c], Bari, Italy
29: Also at Italian National Agency for New Technologies, Energy and Sustainable Economic Development, Bologna, Italy
30: Also at Centro Siciliano di Fisica Nucleare e di Struttura Della Materia, Catania, Italy
31: Also at Scuola Normale e Sezione dell'INFN, Pisa, Italy
32: Also at Riga Technical University, Riga, Latvia, Riga, Latvia
33: Also at Malaysian Nuclear Agency, MOSTI, Kajang, Malaysia
34: Also at Consejo Nacional de Ciencia y Tecnología, Mexico City, Mexico
35: Also at Warsaw University of Technology, Institute of Electronic Systems, Warsaw, Poland
36: Also at Institute for Nuclear Research, Moscow, Russia
37: Now at National Research Nuclear University 'Moscow Engineering Physics Institute' (MEPhI), Moscow, Russia
38: Also at St. Petersburg State Polytechnical University, St. Petersburg, Russia
39: Also at University of Florida, Gainesville, USA
40: Also at Imperial College, London, United Kingdom
41: Also at P.N. Lebedev Physical Institute, Moscow, Russia

42: Also at INFN Sezione di Padova [a], Università di Padova [b], Padova, Italy, Università di Trento [c], Trento, Italy, Padova, Italy
43: Also at Budker Institute of Nuclear Physics, Novosibirsk, Russia
44: Also at Faculty of Physics, University of Belgrade, Belgrade, Serbia
45: Also at Università degli Studi di Siena, Siena, Italy
46: Also at INFN Sezione di Pavia [a], Università di Pavia [b], Pavia, Italy, Pavia, Italy
47: Also at National and Kapodistrian University of Athens, Athens, Greece
48: Also at Universität Zürich, Zurich, Switzerland
49: Also at Stefan Meyer Institute for Subatomic Physics, Vienna, Austria, Vienna, Austria
50: Also at Gaziosmanpasa University, Tokat, Turkey
51: Also at Burdur Mehmet Akif Ersoy University, BURDUR, Turkey
52: Also at Adiyaman University, Adiyaman, Turkey
53: Also at Şırnak University, Sirnak, Turkey
54: Also at Beykent University, Istanbul, Turkey, Istanbul, Turkey
55: Also at Istanbul Aydin University, Application and Research Center for Advanced Studies (App. & Res. Cent. for Advanced Studies), Istanbul, Turkey
56: Also at Mersin University, Mersin, Turkey
57: Also at Piri Reis University, Istanbul, Turkey
58: Also at Ozyegin University, Istanbul, Turkey
59: Also at Izmir Institute of Technology, Izmir, Turkey
60: Also at Marmara University, Istanbul, Turkey
61: Also at Kafkas University, Kars, Turkey
62: Also at Istanbul Bilgi University, Istanbul, Turkey
63: Also at Hacettepe University, Ankara, Turkey
64: Also at Vrije Universiteit Brussel, Brussel, Belgium
65: Also at School of Physics and Astronomy, University of Southampton, Southampton, United Kingdom
66: Also at IPPP Durham University, Durham, United Kingdom
67: Also at Monash University, Faculty of Science, Clayton, Australia
68: Also at Bethel University, St. Paul, Minneapolis, USA, St. Paul, USA
69: Also at Karamanoğlu Mehmetbey University, Karaman, Turkey
70: Also at Vilnius University, Vilnius, Lithuania
71: Also at Bingol University, Bingol, Turkey
72: Also at Georgian Technical University, Tbilisi, Georgia
73: Also at Sinop University, Sinop, Turkey
74: Also at Mimar Sinan University, Istanbul, Istanbul, Turkey
75: Also at Nanjing Normal University Department of Physics, Nanjing, China
76: Also at Texas A&M University at Qatar, Doha, Qatar
77: Also at Kyungpook National University, Daegu, Korea, Daegu, Korea
78: Also at University of Hyderabad, Hyderabad, India